Establishing Fluid Dynamics Scales Critical to Dynamic Interface Applications and their Impact on Handling Qualities

Quarterly Status Report 10

Period of Performance: 6/5/2023 – 9/4/2023

Prepared by:

G. R. Whitehouse
Continuum Dynamics, Inc.
34 Lexington Avenue
Ewing, NJ 08618-2302

Prepared for:

David Gonzalez
Office of Naval Research
875 North Randolph
Street
Arlington VA 22203

Under Contract No. N00014-21-C-1044

Glen R. Whitehouse

September 13, 2023

Project Summary

One of the most demanding tasks for naval aviators is landing on a moving flight deck in high sea-states (i.e. the dynamic interface (DI) problem - see Figure 1). This task is made even more difficult by aerodynamic disturbances at the landing spot from the flow around the ship's bow, superstructure and deck edges. This highly unsteady ship airwake can lead to significant pilot workload. Flight simulation has long been recognized as a valuable tool for augmenting engineering development and pilot training in DI operations, however, it is most effective when the underlying simulation model has appropriately characterized the complex aerodynamic interactions between the rotorcraft and ship airwake. Given the complexity of the problem, a fundamental difficulty when assessing the simulation approaches is the quantification of "good enough", both from the standpoint of understanding and predicting the underlying physics and also with regards to trainer fidelity (i.e. can the pilot feel/tell a difference). The premise of the proposed effort is to quantify "good enough" with regards to understanding the fundamental aero-physics of a rotorcraft interacting with an external disturbance field to quantify which length and time scales - such as those present in a ship airwake or in the wake of a an upstream aircraft during formation flight/refueling - directly impact the aircraft's fundamental response and flying qualities (FQ) along with the aeromechanics modeling fidelity required to simulate interactions adequately.

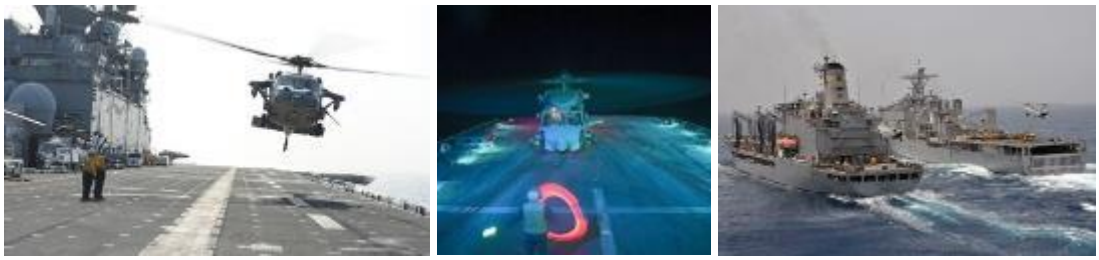

Figure 1: DI scenarios: landing on a moving deck (left), night operations (center) and approaching a pair ships (right)

Several ONR funded efforts that seek to quantify "good enough" have recently completed, or are underway, at the University of Maryland, Georgia Institute of Technology and NAVAIR, where the academic researchers are focusing on understanding the response of a wing to the wake shed by canonical structures [1] and the latter (Generalized Airwake Goodness Evaluation) program seeks to represent the entire DI scenario with a variety of methods. This effort does not seek to duplicate that work, rather to complement it by focusing on several fundamental unknowns in the rotorcraft community, namely:

1. What spatial and temporal scales, present in a disturbance field, matter from Flight Dynamics (FD) and FQ standpoints? Beyond the obvious constraints (i.e. larger than a rotor radius and those that induce velocities larger than the wake induced velocity), how does a rotor respond to different size disturbances and how does the rotor type influence this? For example, in general, a rotor acts to filter the influence of a disturbance field, but the level of filtering will vary significantly between an articulated flexible rotor (H-60) and a gimballed stiff one (V-22). Moreover, rotors typically respond ~90^o out of phase of the disturbance, whereas fixed aerodynamic surfaces response directly in-phase, which results in a fundamentally different response between rotorcraft types (i.e. helicopter vs. tiltrotor).

2. How do these scales vary when the effects on the full aircraft are accounted for? The primary response from the helicopter will be dominated by that of the rotor, though there may still be significant response associated with the disturbance induced flow on the fuselage, empennage and tail rotor.
3. How do these scales vary with aircraft configuration/type (i.e. conventional helicopter vs. tiltrotor)? The primary response from the helicopter will be dominated by that of the rotor, whereas the tiltrotor may respond primarily in a fixed wing manner associated with the induced flow on the wing. Of course, the tiltrotor's response will also vary with nacelle angle, and it is well known that the V-22's response to wake disturbances (i.e. during formation flight) is quite different to other rotorcraft in the Navy's inventory [2].
4. How do these scales vary with aircraft flight condition, and can valid modeling simplifications be made (i.e. distorting vs. classical frozen disturbance field)? Work by Whitehouse and Brown for helicopter rotors [3-7] suggests that for high speed flight, the traditional frozen field (superposition) assumption may be adequate, but that at the low speeds associated with DI operations, a distorting disturbance field and wake are required because the response is critically different.

Developing an understanding of fundamental aircraft aeromechanic response, FD, and FQ to the unknowns outlined above would provide great utility to the community with regards to establishing the level of modeling fidelity required to accurately simulate disturbance interactions, the level of fidelity required to be output by CFD simulation generated ship airwake databases for training scenarios, and the quantification and specification of handling qualities to types of disturbance fields that can be used to define future and ongoing training and aircraft performance requirements and specifications, such as ADS-33 [8].

Technical Objectives

The goal of the effort is to develop a fundamental understanding of the relationship between the length and time scales typically present in disturbance fields experienced by Naval aviators (i.e. ship airwakes, wing wakes etc.) and rotorcraft FD and FQ when the fully-interacting fluid dynamics of the airwake and rotor wake and flight mechanics are accounted for. With this information in hand, the engineering community would be better able to understand the relationship between aircraft type, ride quality, FD and FQ during flight conditions where disturbance fields are encountered. The community would be able to more accurately define trainer requirements, minimum experimental campaign requirements, minimum CFD modeling requirements and consequently establish a benchmark to evaluate CFD predictive capability. Furthermore, the conclusions of this work would also directly impact the development of requirements for new aircraft given the direct correlation between FD and FQ. The proposed effort would undertake the research required to develop such an understanding, with disseminating the observations and conclusions of the work to the Navy and the broader FD, FQ and handling qualities communities - a key objective from the outset. The effort will be structured using a build-up approach that first focuses on defining relevant disturbance fields followed by predicting and understanding the fundamental aeromechanics response (i.e. aerodynamic forces and moments and rotor dynamics). The effort would culminate in predicting the flight dynamics and handling qualities for realistic, but generic, helicopter and tiltrotor configurations that include representations of flight controls, propulsion system and cross-

coupling characteristics. The key objectives for the effort roughly form the main tasks and are as follows:

1. Define the spatial and temporal fluid dynamic scales present in relevant disturbance fields and develop numerical representations for testing (Year 1).
2. 6-DOF generic model assembly and shakedown testing to ensure correct operation and functionality.(Year 1)
3. Define aeromechanics performance and HQ metrics along with a detailed simulation test matrix that includes systematic and consistent model fidelity build-up (Year 1-2).
4. Undertake simulation of a generic helicopter interacting with frozen and distorting disturbance fields to establish fundamental response characteristics (Year 2).
5. Undertake simulation of a generic tiltrotor interacting with frozen and distorting disturbance fields to establish fundamental response characteristics (Year 2).
6. Develop a realistic full helicopter model and undertake simulations of interactions with frozen and distorting disturbance fields to establish flight dynamics and handling qualities response (Year 3).
7. Develop a realistic full tiltrotor model and undertake simulations of interactions with frozen and distorting disturbance fields to establish flight dynamics and handling qualities response (Year 3).
8. Documentation and dissemination of observations and conclusions to the Navy and the wider FD/HQ community (Years 1-3).

Summary of Work Conducted During Reporting Period

Work during the present reporting period has focused on the characterization of additional flow features associated with headwind over a cube, their scalability and applicability to a representative ship geometry, and their influence on idealized rotors along an approach trajectory that is representative of actual piloted trajectories. Corrections to the analytical rotor response expressions presented in the previous progress report were made and are presented. The characterization of flow features associated with a headwind flow over a cube and the parametrization employed to develop two generic classes of ship geometries is presented. The scalability of the flow features to one of these generic ship geometries is investigated along with the fundamental responses of idealized rotors representative of the MQ-8C FireScout, UH-60A, V-22 and CH-53E rotorcraft in an approach trajectory.

In addition, a presentation was given at the 2023 ONR Annual Aerodynamics Program Review, and a copy of the slides provided below for reference.

Quantifying Fundamental Influence of Wake Structures on Rotorcraft (Corrections to Previous Progress Report)

The influence of an arbitrary vortex wake structure on the fundamental response of a rotor can be derived using BET analysis [5, 7]. Detailed derivation of these equations is provided in Ref. [7]. We focus here on the assumptions made and resulting expressions.

Consider an “idealized” rotor with the following assumptions:

- No hub accelerations;
- Controls remain fixed;

- No hinge offset;
- Quasistatic response whereby the flap response of the rotor is much faster than the speed at which the vortex structure traverses the rotor; and
- Only the vertical component of the velocity associated with the arbitrary vortex is considered since it directly influences rotor inflow.

The influence of an arbitrary vortex with nondimensional vertical velocity $v_{vortex}(r,\psi)$, where r is the radial coordinate and ψ is the rotor azimuth, on rotor thrust coefficient C_T, coning β_0, lateral disc tilt β_{1s} and longitudinal disc tilt β_{1c} is given by the following expressions [7]:

$$C_T = C_T^* - \frac{Nca}{4\pi^2}\int_0^{2\pi}\int_0^1 v_{vortex}(r,\psi)(r+\mu\sin\psi)dr\,d\psi,$$

$$\beta_0 = \beta_0^* - \frac{ca}{4\pi^2\omega^2 I_\beta}\int_0^{2\pi}\int_0^1 v_{vortex}(r,\psi)(r^2+\mu r\sin\psi)dr\,d\psi, \quad (1)$$

$$\beta_{1s} = \beta_{1s}^* + \frac{ca}{2\pi^2(\omega^2-1)I_\beta}\int_0^{2\pi}\int_0^1 v_{vortex}(r,\psi)(r^2\sin\psi+\mu r\sin^2\psi)dr\,d\psi,$$

$$\beta_{1c} = \beta_{1c}^* + \frac{ca}{2\pi^2(\omega^2-1)I_\beta}\int_0^{2\pi}\int_0^1 v_{vortex}(r,\psi)(r^2\cos\psi+\mu r\cos\psi\sin\psi)dr\,d\psi,$$

where $(\,)^*$ terms represent the responses without the vortex, N is the number of rotor blades, a is the airfoil lift-curve slope, c is the blade chord length nondimensionalized by rotor radius R, ω is the flap natural frequency nondimensionalized by rotor rotational speed Ω ($\omega = 1$ for zero hinge offset), and I_β is the blade flapping inertia nondimensionalized by ρAR^3, where ρ is air density, A is the rotor disc area. For a specified vortex velocity function $v_{vortex}(r,\psi)$, the corresponding influence on rotor fundamental response can therefore be quantified using the expressions in Eq. (1).

Rotor Fundamental Response

In the prior report we derived a velocity model for the arch vortex that develops aft of rectangular obstacles in headwind flow. This model is equivalent to the function $v_{vortex}(r,\psi)$ from Eq. (1) and enables the computation of fundamental rotor response to the airwake velocities associated with the arch vortex. For the fundamental response analysis, we consider rotors representative of four helicopters as summarized in Table 1 and Figure 2. The expressions in Eq. (1) are evaluated using the rotor properties from Table 1 and the arch vortex model vertical velocity predictions obtained using Eq. (1). We consider two locations for the rotor hub center in our analyses: [x,y,z] = [0, 8, -20]m (location #1) and [x,y,z] = [0, 6, -25]m (location #2), both defined relative to the coordinate system shown in Figure 3.

Table 1: Rotor properties considered in fundamental response analysis. (Please note that given the similarity between the rotor systems, the UH-60A specifications are used for the SH-60)

Vehicle	**Number of blades**	**Chord [ft]**	**Radius [ft]**	**Rotation speed [rad/s]**	**GW [lbs]**	**Ibeta [slug-ft2]**
MQ-8C Fire scout (Bell 407)	4	0.9	17.5	43.25	5400	143.8
SH-60/UH-60A	4	1.73	26.83	27	16500	1512.6
V-22	3	2.09	19	41.57	39500	721.6
CH-53E	7	2.44	39.5	18.53	60000	6744.7

Figure 2: Aircraft used as the basis of rotor response analysis: (top left) MQ-8C Fire scout (Bell 407); (top right) Sikorsky SH-60; (bottom left) Bell/Boeing V-22, and (bottom right) Sikorsky CH-53E

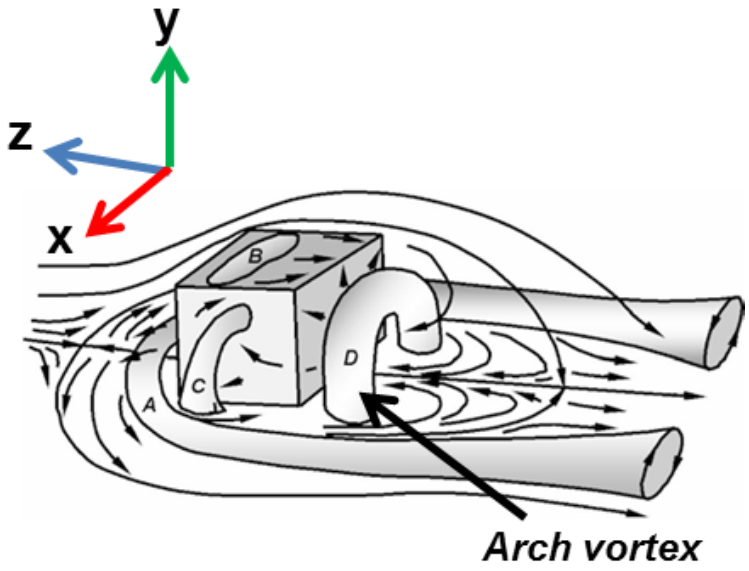

Figure 3: Reference frame and principal flow features around surface-mounted obstacle, adapted from [9]

The magnitude of the arch vortex influence on the thrust coefficient (C_T) and longitudinal disk tilt (β_{1c}) on different rotors is depicted in Figure 4 and Figure 5 (the change in lateral disk tilt (β_{1s}) is negligible, and is thus not shown here) for hover ($\mu = 0$). Points that lie furthest from the origin indicate the strongest influence. At location #1, the influence of the arch vortex on the smaller MQ-8C rotor is strongest, followed in order of decreasing influence by the UH-60A rotor, the V-22 rotor and the CH-53E rotor. At location #2, the MQ-8C is again the most affected rotor, but this time, we note a greater arch vortex influence on the responses of UH-60A and CH-53E rotors. The influence of ship airwake flow features on rotor responses is thus characterized by both rotor properties (size, number of blades etc.) and position. Contours of velocity predictions using the arch vortex model and CGE/VorTran-M over the MQ-8C and CH-53E rotors (smallest and largest rotors considered, respectively) at locations #1 and #2 are shown in Figure 6 and Figure 7, respectively, for reference. Reasonable agreement in velocity predictions is noted with the largest discrepancies noted for the vertical velocity predictions, as was noted previously as well.

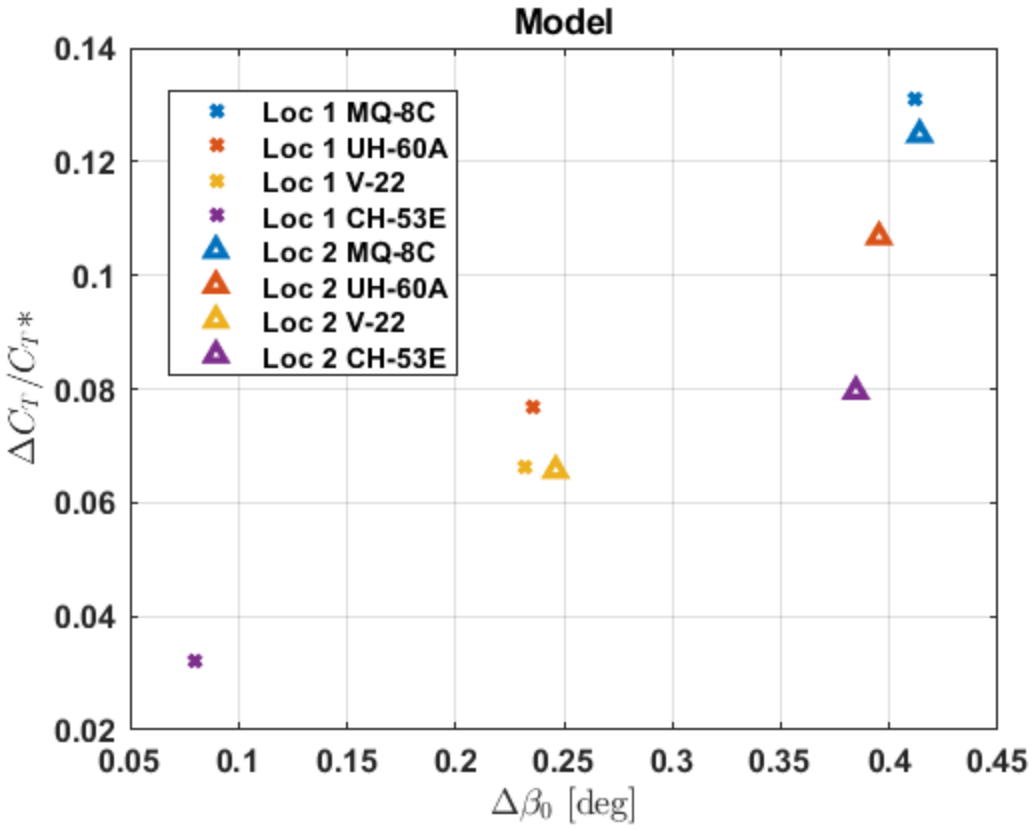

Figure 4: Influence of arch vortex on rotor fundamental response; $C_T^* = W/\rho(\pi R)^2(\Omega R)^2$, $\Delta C_T = C_T - C_T^*$, $\Delta\beta_0 = \beta_0 - \beta_0^*$.

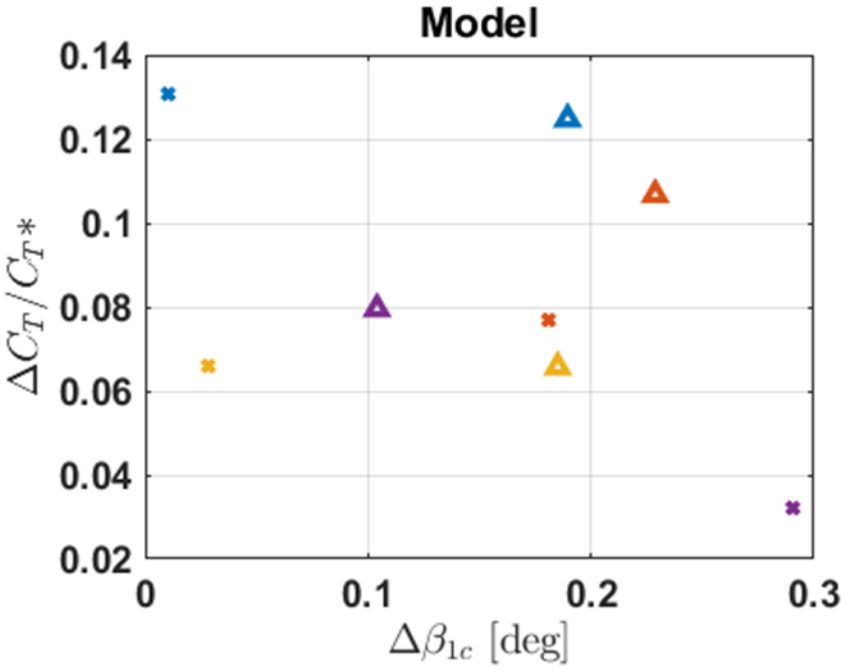

Figure 5: Influence of arch vortex on rotor longitudinal disk tilt; $C_T^* = W/\rho(\pi R)^2(\Omega R)^2$, $\Delta C_T = C_T - C_T^*$, $\Delta\beta_{1c} = \beta_{1c} - \beta_{1c}^*$.

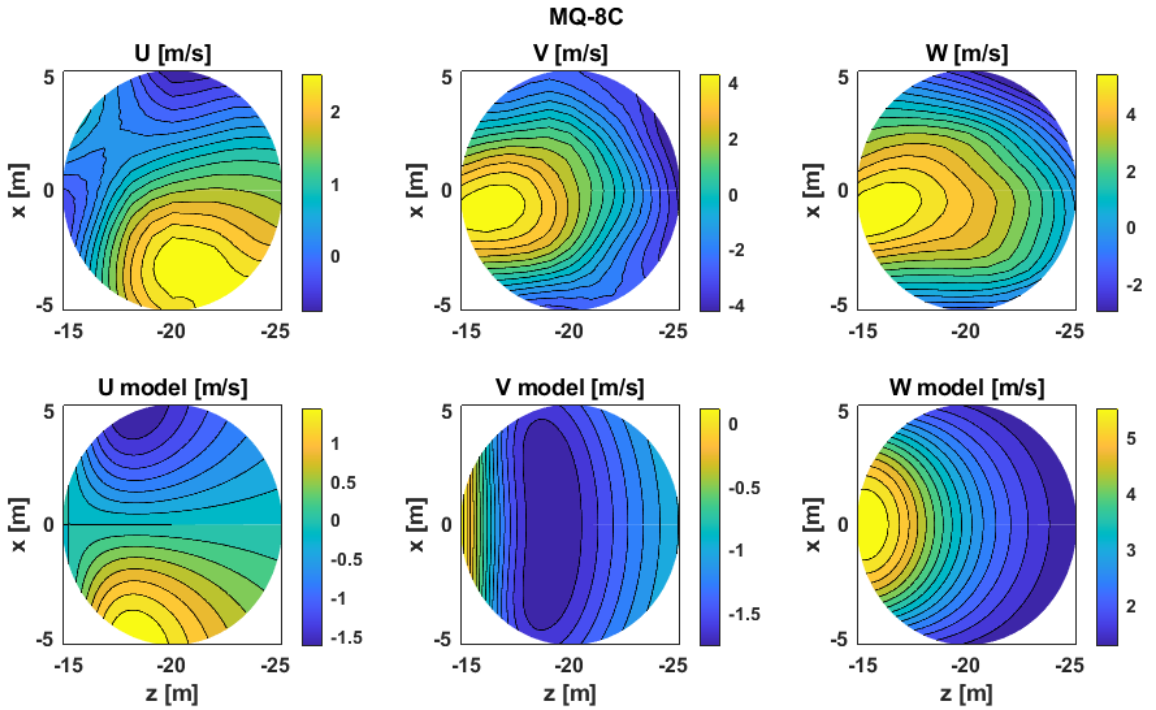

(a)

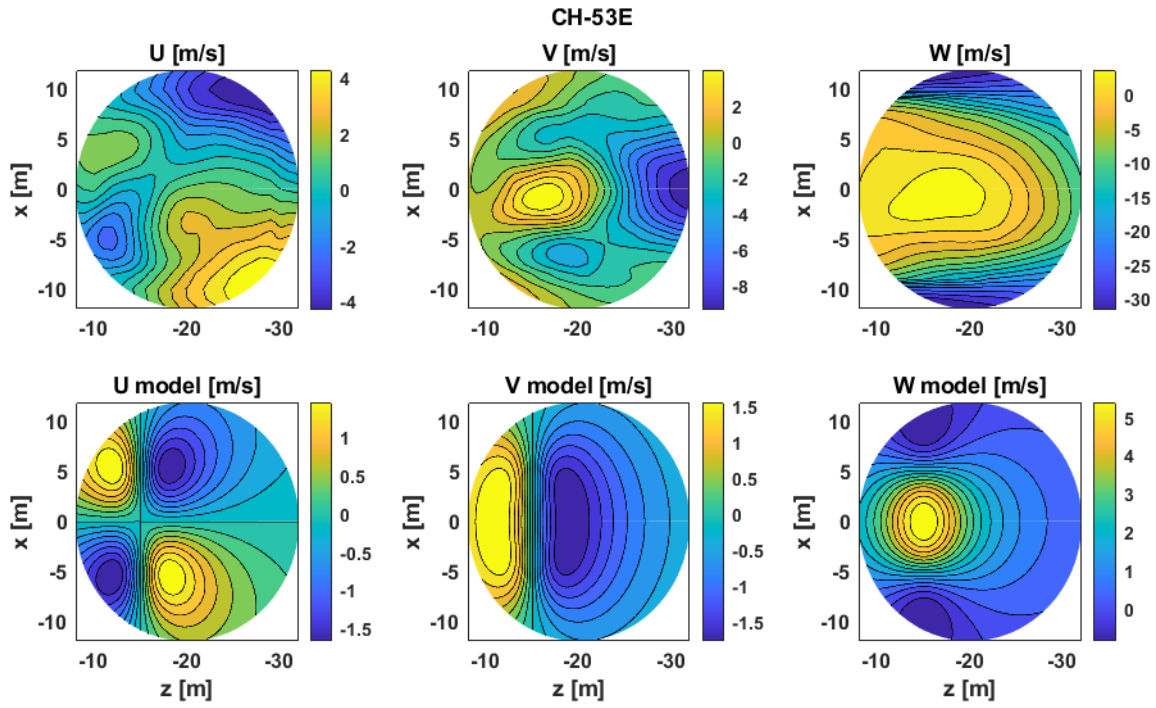

(b)

Figure 6: Contours of airwake velocity components over MQ-8C and CH-53E rotor centers at location #1 where [x,y,z] = [0, 8, -20]m.

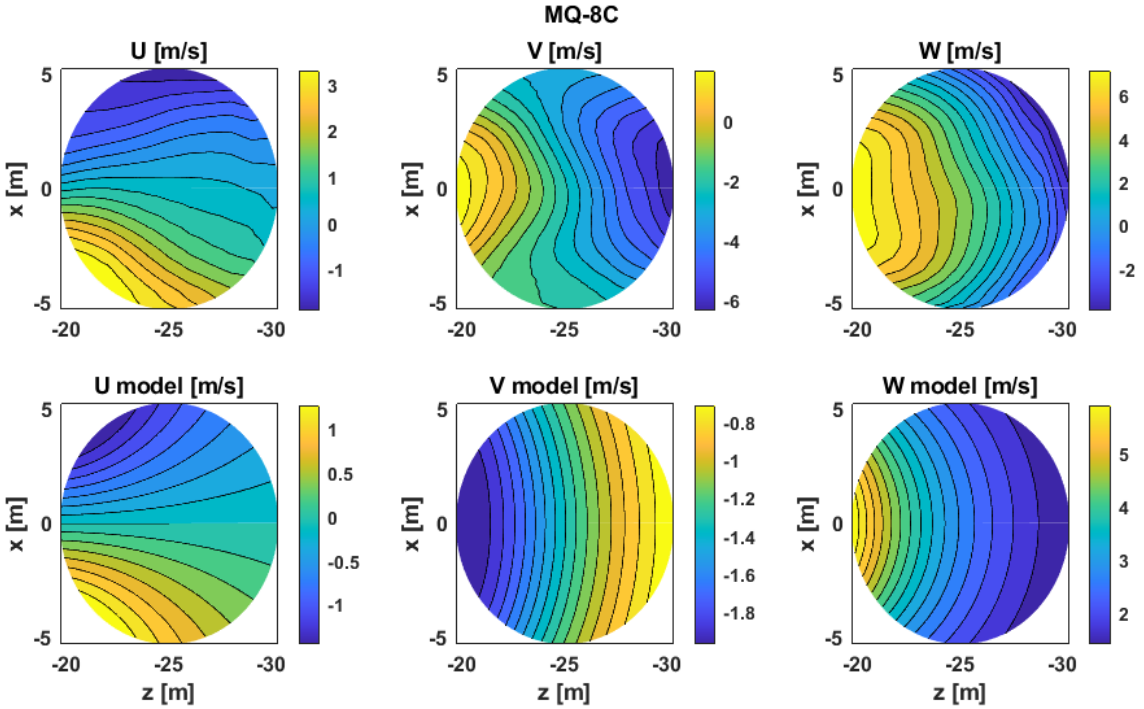

(a)

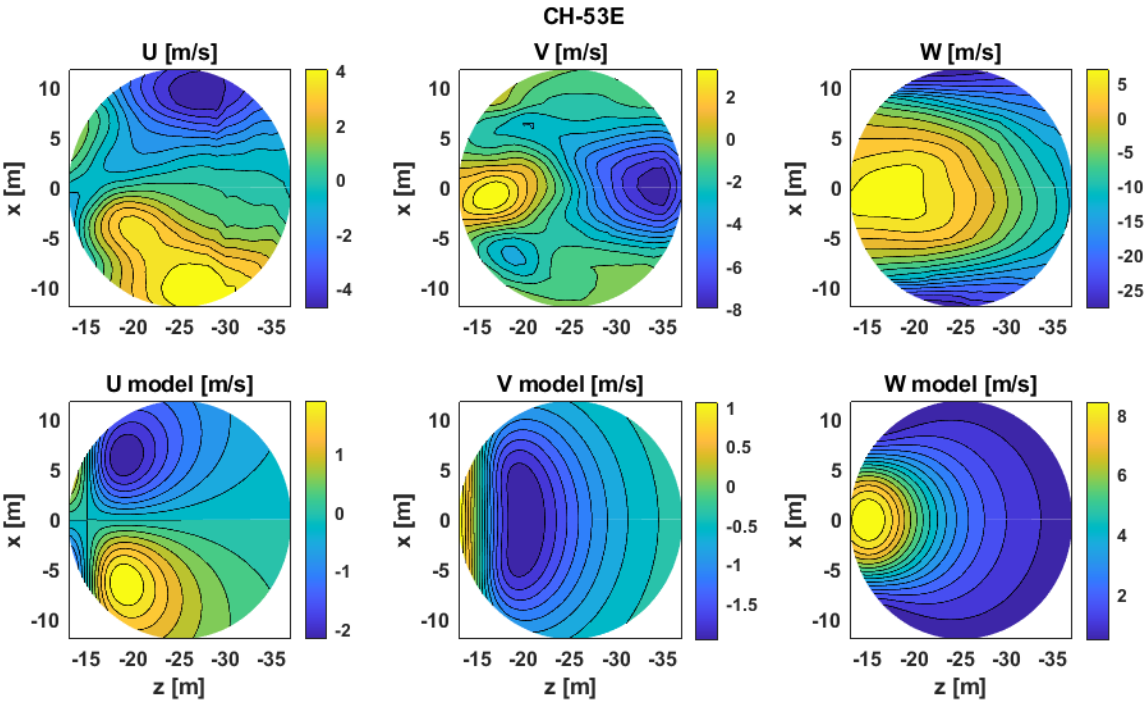

(b)

Figure 7: Contours of airwake velocity components over MQ-8C and CH-53E rotor centers at location #2 where [x,y,z] = [0, 6, -25]m.

Flow Feature Characterization

Headwind Over Cube

Flow over a simple cube, which represents a canonical shape, was considered to start off. Primary flow features reported in literature are shown in Figure 3 and include:

- A horseshoe vortex that forms upstream of the obstacle where the flow stagnates and wraps around the cube (feature "A" on the figure);
- On the top and side surfaces, local separation and reattachment regions ("B" and "C" on the figure);
- In the lee of the obstacle, an arch vortex (feature "D" on the figure) that forms due to the separation of the shear layers from the top and side surfaces. The streamlines aft of the obstacle indicate a recirculation region, where the direction of the flow reverses.

We identified these flow features in our CFD simulations as well. Note that all position coordinates are expressed relative to the reference frame shown in the Figure, which has its origin at the center of the bottom face of the geometry. Additionally, all the characterization considered thus far is based on time-averaged velocity data.

The flow structures are vortical structures that can be characterized in terms of *geometry* (position and size) and *strength* (circulation). In the prior report, we carried out geometry and strength characterization for the arch vortex shown in Figure 3. The steps involved in the characterization consisted of:

1. Plotting the velocity field along multiple 2D planes as a quiver plot to locate vortex centers;
2. Ensuring any rotational behavior observed corresponded to a vortex by cross-checking with corresponding Q-criterion and Δ-criterion contour plots;
3. Picking out the vortex center position and the position where maximum tangential velocity is noted (the latter demarked the vortex core limit);
4. Computing the circulation associated with the region that encloses the vortex;
5. Nondimensionalizing the position coordinates of the vortex core center and core radius size along the different planes by an obstacle dimension (e.g., height) and the circulation by the product of an obstacle dimension and free stream speed; and
6. Fitting polynomial expressions on the nondimensional vortex center position and radius data.

To test out the characterization, we implemented a numerical vortex model that combined the Biot-Savart law with the Vatistas viscous core model to obtain associated induced velocity predictions, which were then compared with CFD velocities. The velocity induced at position $\boldsymbol{r}$ relative to a discretized vortex filament element $\boldsymbol{dl}$ was given by

$$\boldsymbol{V}_{ind} = \frac{\Gamma h}{4\pi(r_c^{2n} + h^{2n})^{1/n}} \int \frac{d\boldsymbol{l} \times \boldsymbol{r}}{|\boldsymbol{r}|^3} \times fac, \tag{2}$$

where Γ is the vortex circulation (strength), h is the perpendicular distance of the evaluation point from the vortex filament element, n is an integer that controls the smoothness of the transition of the velocity predictions from the viscous core to the external inviscid region (we

used $n = 1$), and fac is a scaling factor that was needed for accurate predictions. The arch vortex was represented as a parabolic vortex filament with a ground mirror counterpart in this formulation. We had found reasonable agreement with CFD predictions for the lateral u and longitudinal w velocity components.

During the present reporting period, we performed flow feature characterization for additional flow structures.

Aft of the obstacle, carrying out the steps listed above for z=constant planes revealed the existence of two symmetrical vortical tubes downstream of the obstacle. These vortical structures are likely associated with the interaction of the shear layers shed from the side, top and corner edges of the cube. We modeled these flow structures as a horseshoe vortex with the following limits: $x \in [-0.5,0.5]W$, $y = 0.9H$ and $z \in [1.5,\infty]H$ downstream, where W is the obstacle width and H the obstacle height. The nondimensional circulation was found to be 0.01. To test out the characterization, we performed velocity reconstruction using Eq. (2) with $fac = 15$, determined manually. Resulting velocity contours, together with from CFD simulations are plotted in Figure 8 for various z=constant planes. Note that the CGE/VorTran-M (CFD) predictions include influence from all flow features and that the horseshoe filament vortex has its horizontal part at z=-20m. Good agreement in the vertical v velocity profiles is noted downstream from approximately $z = -24$m onwards. Closer to the obstacle at z=-18m, which is in the fore region of the horseshoe vortex, the model underpredicts the vertical velocity. The trends exhibited by the lateral u velocity contours bear some resemblance to those from CFD simulations in all the plots, while a mismatch is noted in the longitudinal w velocity ones. The results here are promising given that the vertical velocity of the airwake is the component that directly influences rotor inflow and is reasonably captured using an isolated horseshoe vortex.

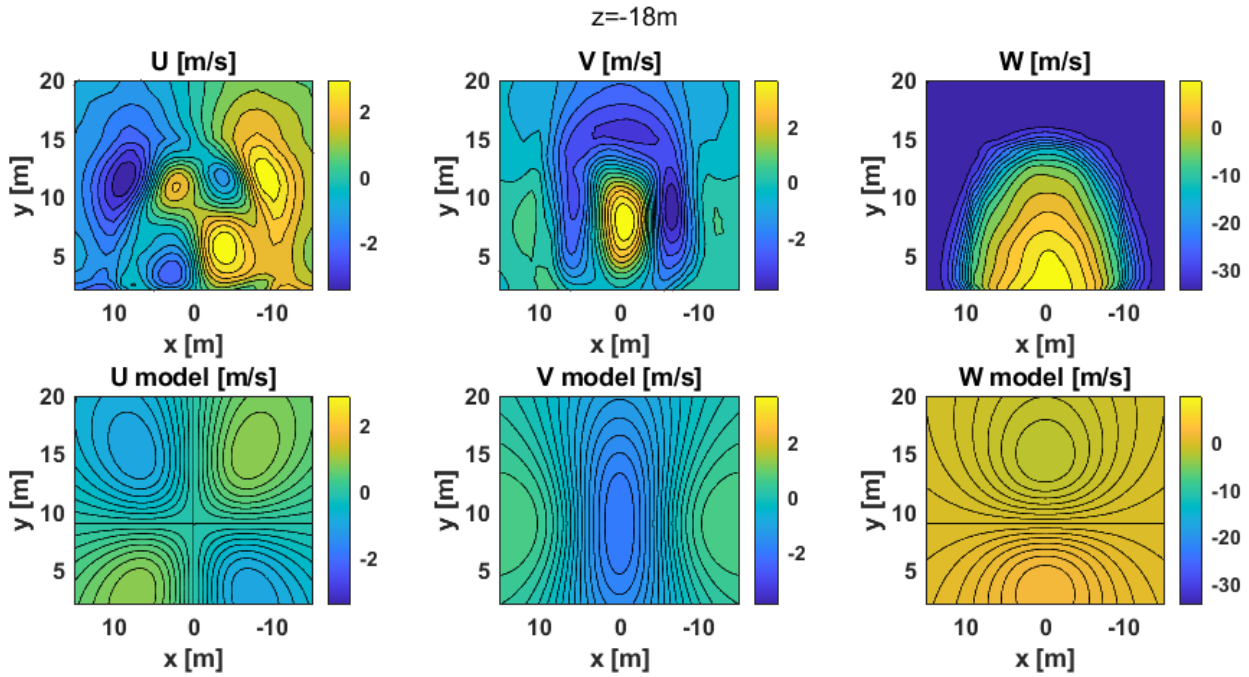

(a)

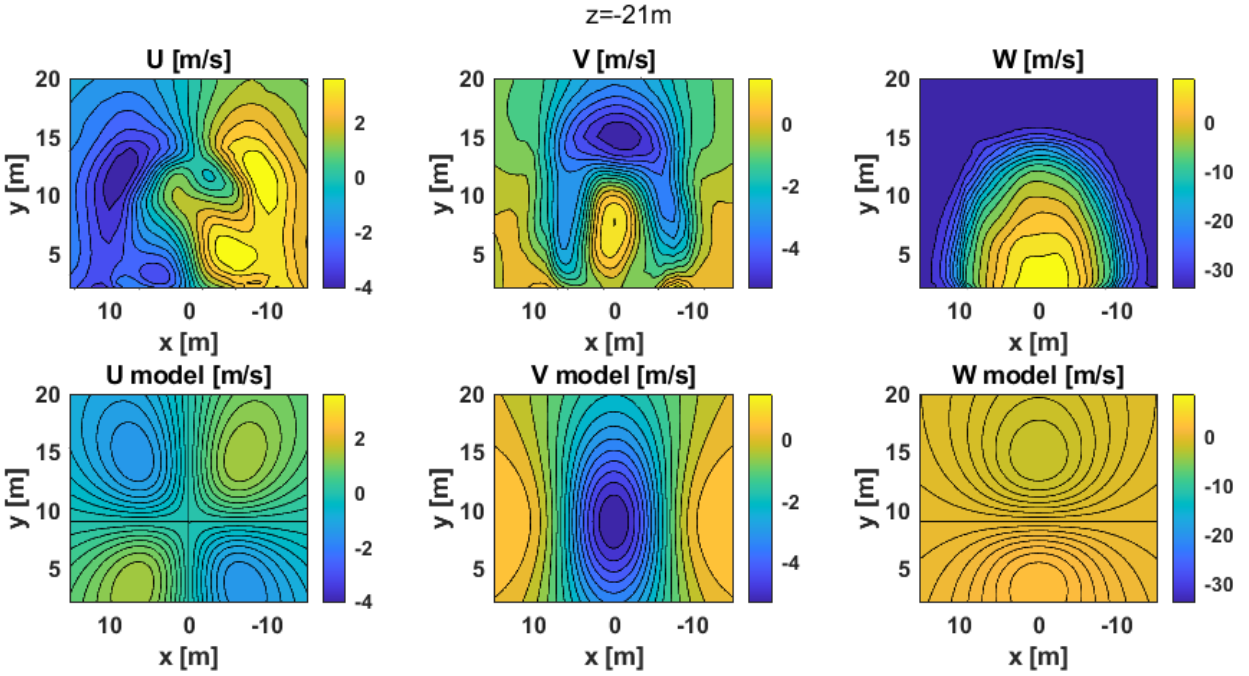

(b)

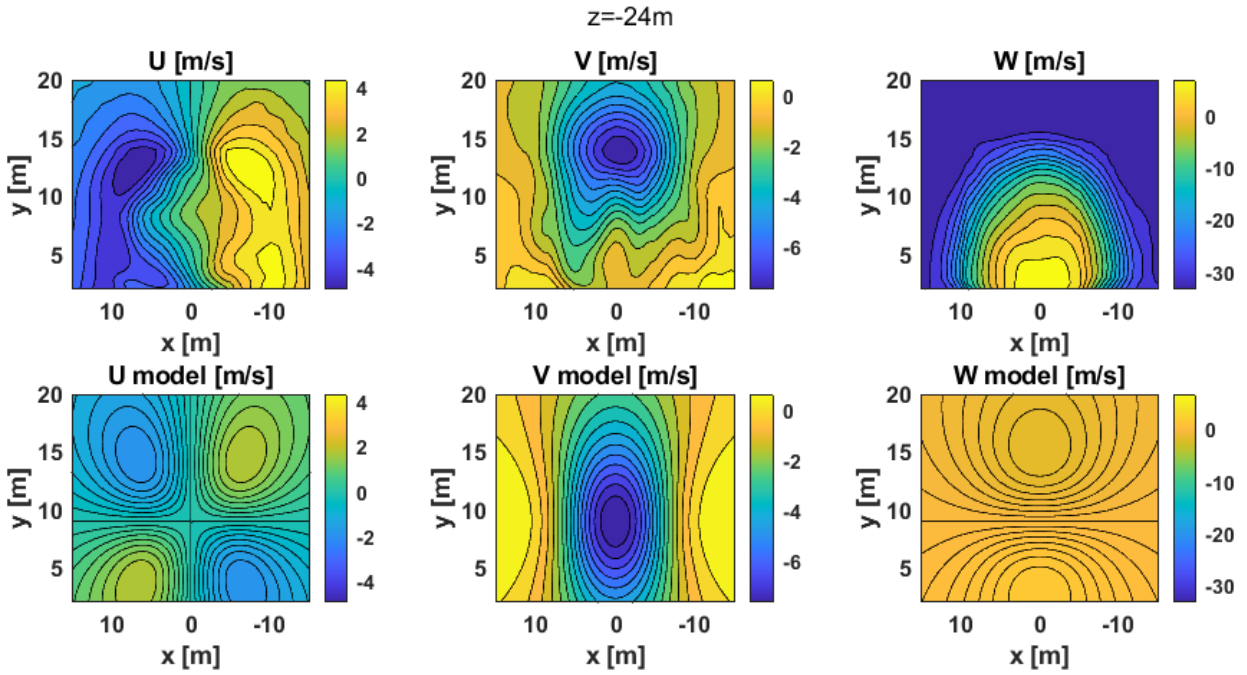

(c)

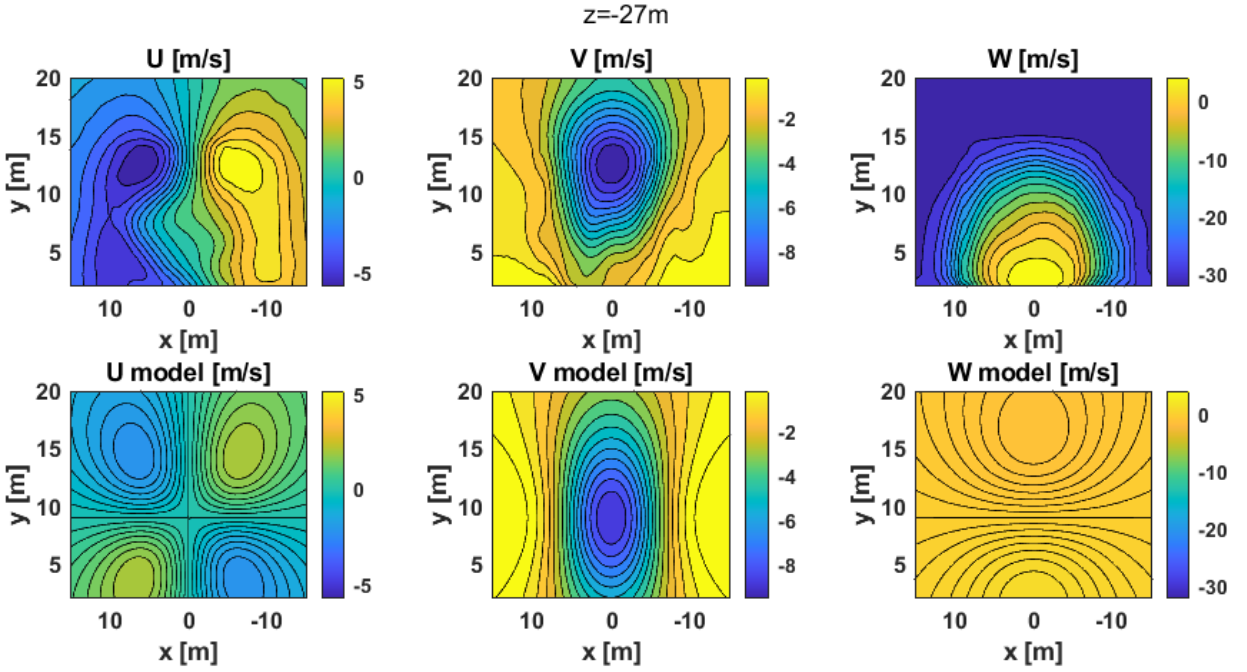

(d)

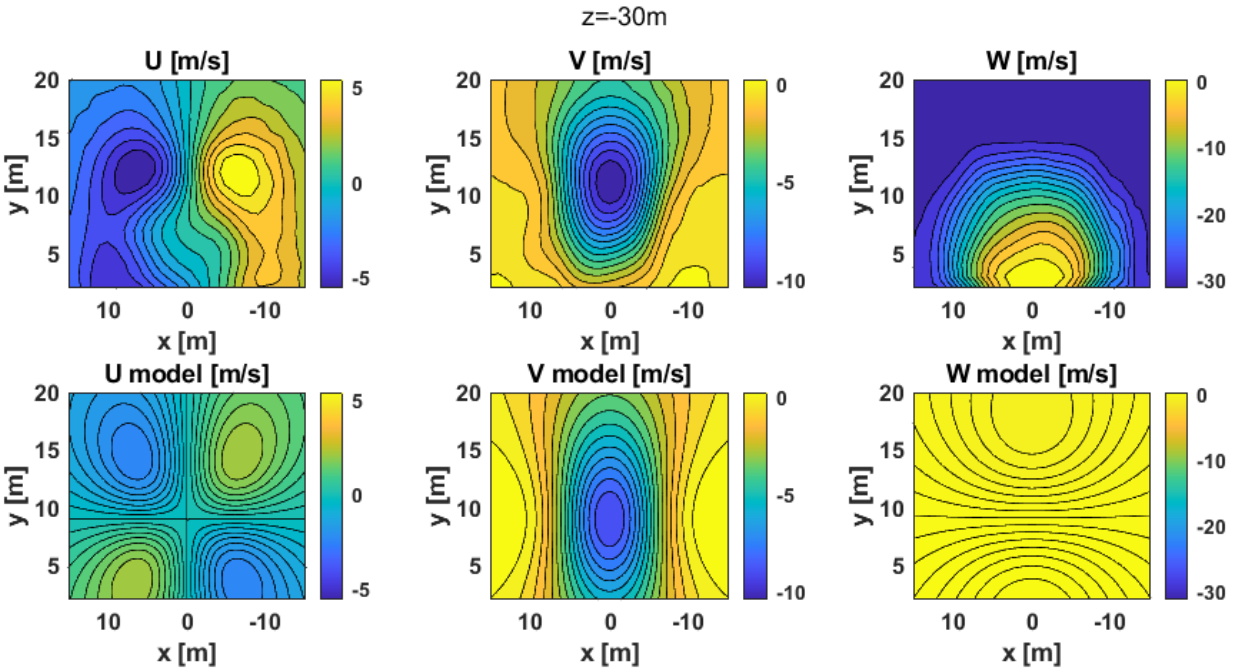

(e)

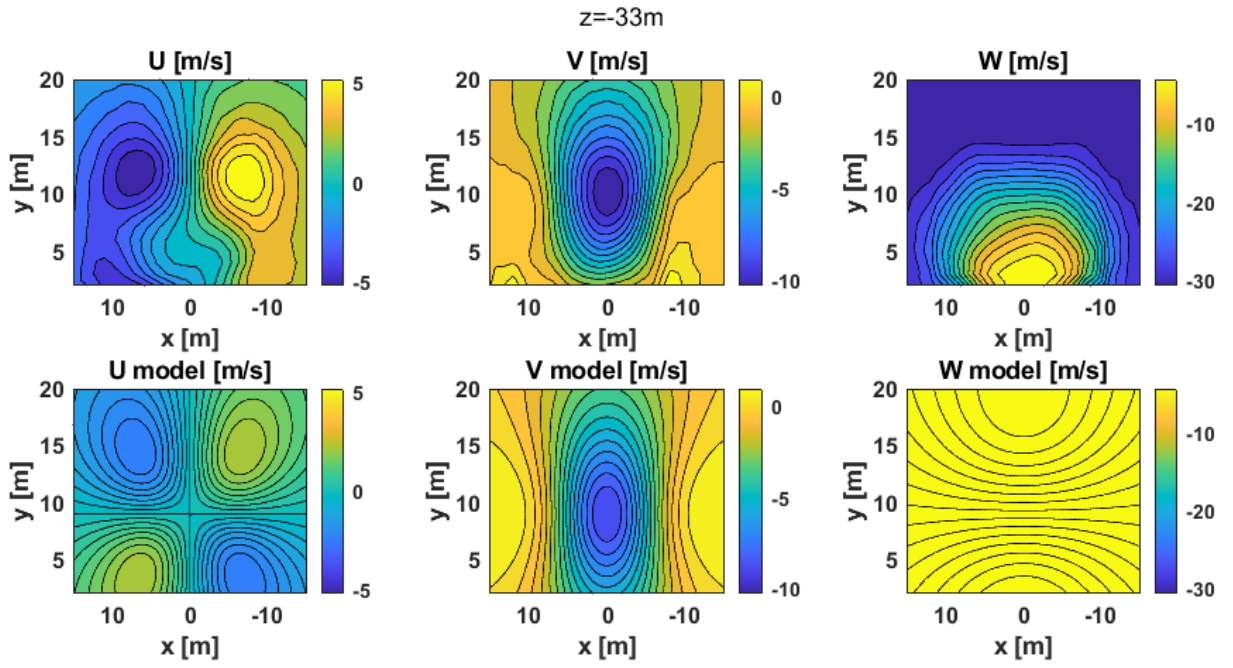

(f)

Figure 8: Contours of airwake velocity components aft of the 10m cube for various z=constant planes obtained using CGE/VorTran-M and aft horseshoe vortex model.

The combined (superimposed) influence of the arch vortex from the previous progress report and the horseshoe vortex is considered in Figure 9, where associated velocities at various z=constant planes are plotted. From the Figure, the inclusion of the arch vortex model improves longitudinal *w* velocity predictions below y=10m up to approximately z=-27m downstream.

Lateral u velocity predictions, however, are seen to have a lower magnitude than the counterparts in Figure 8. The vertical velocity profiles in Figure 9 are similar to those from Figure 8, indicating that contributions from the horseshoe vortex are dominant.

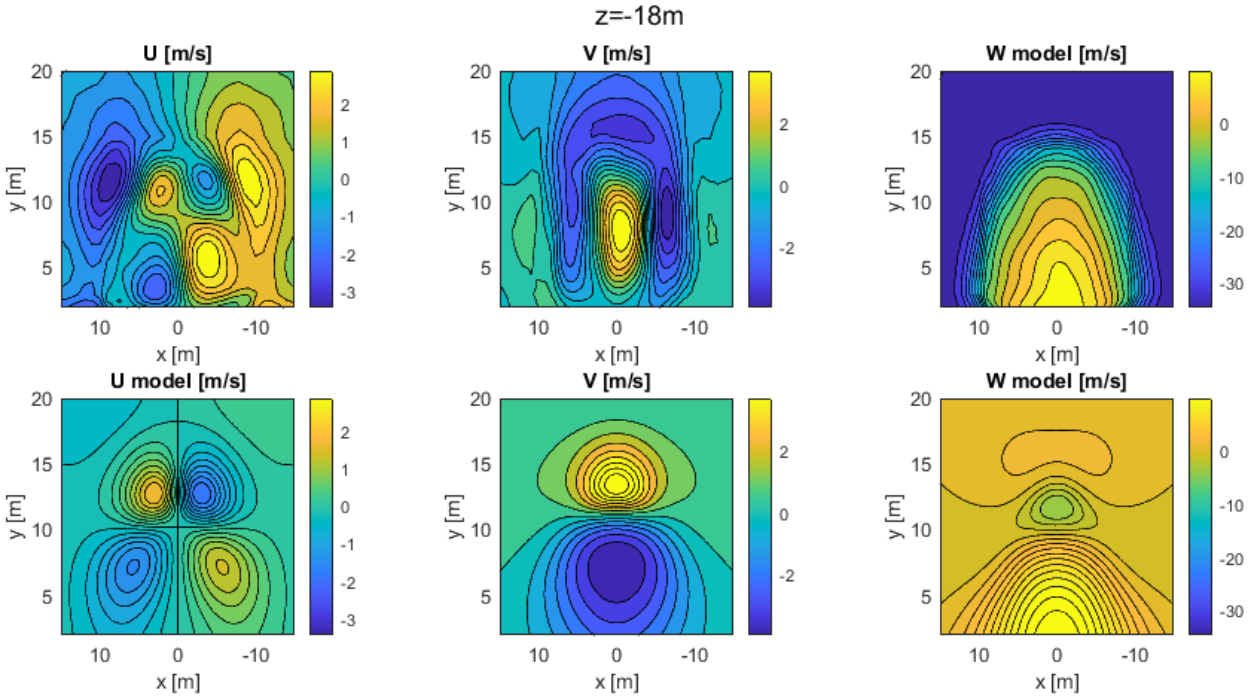

(a)

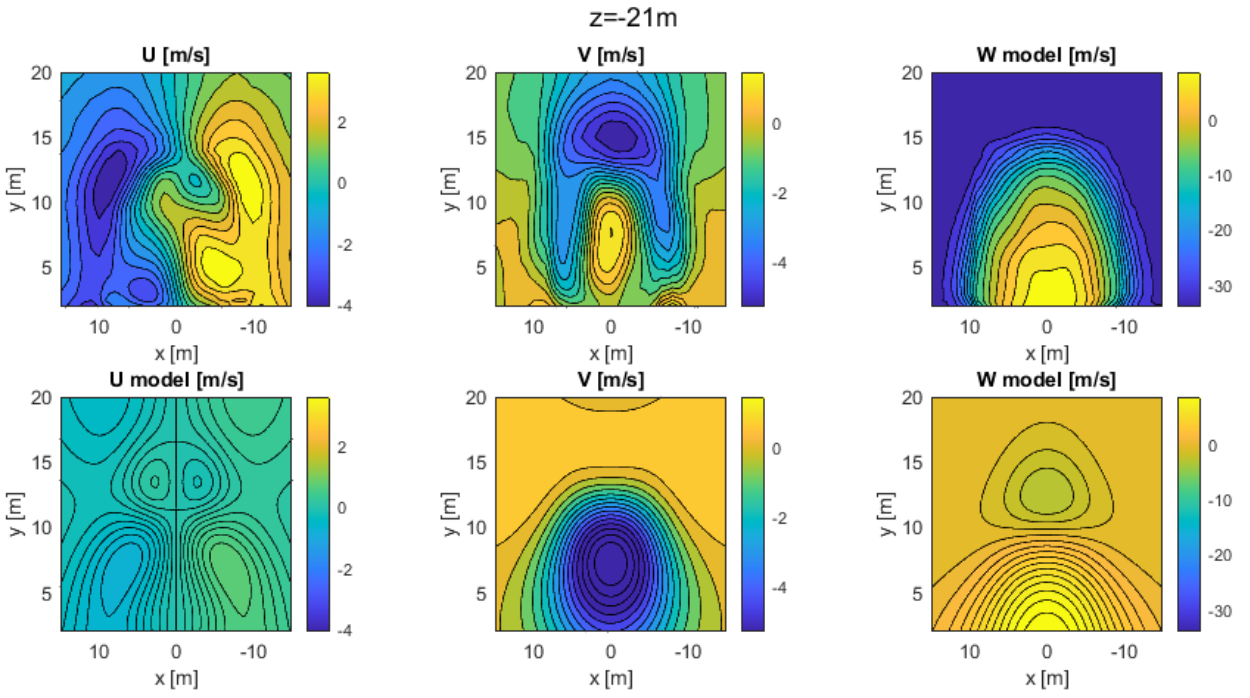

(b)

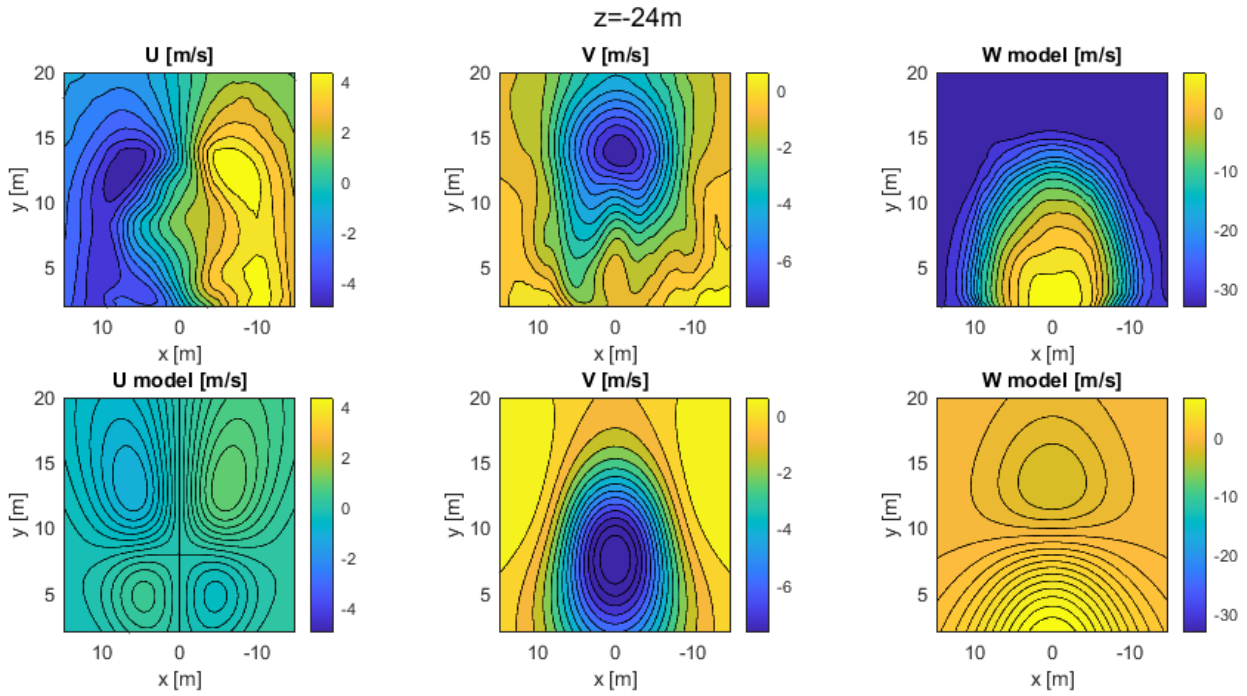

(c)

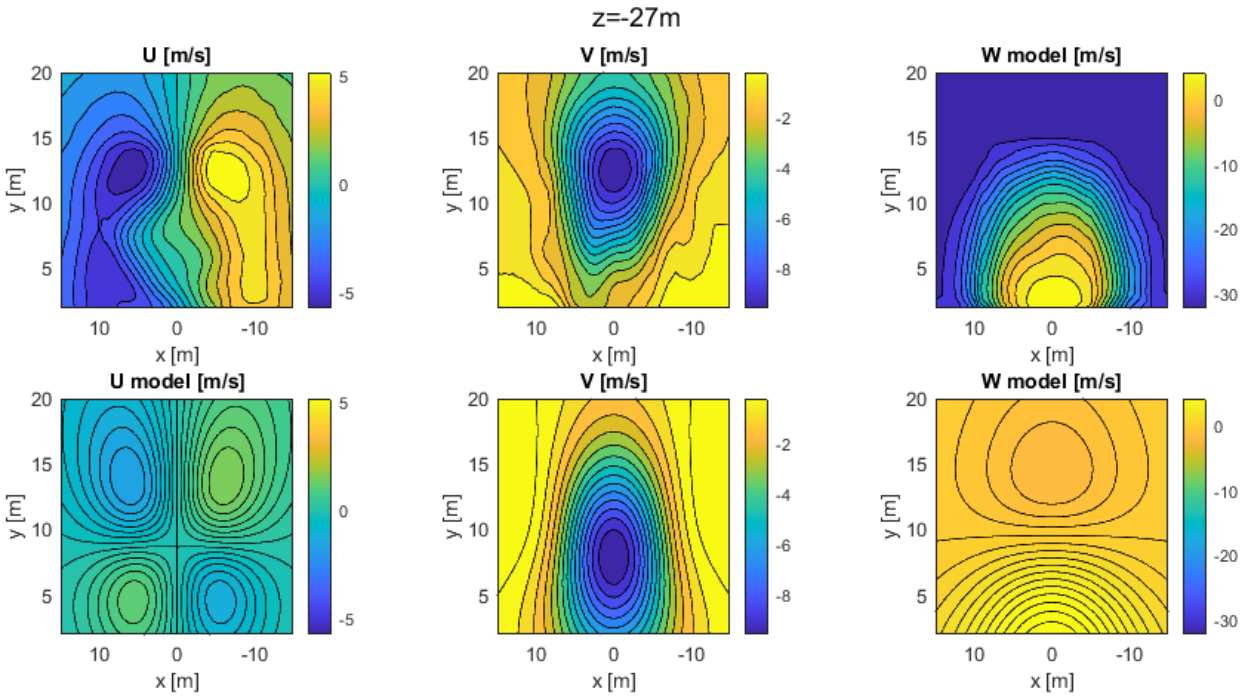

(d)

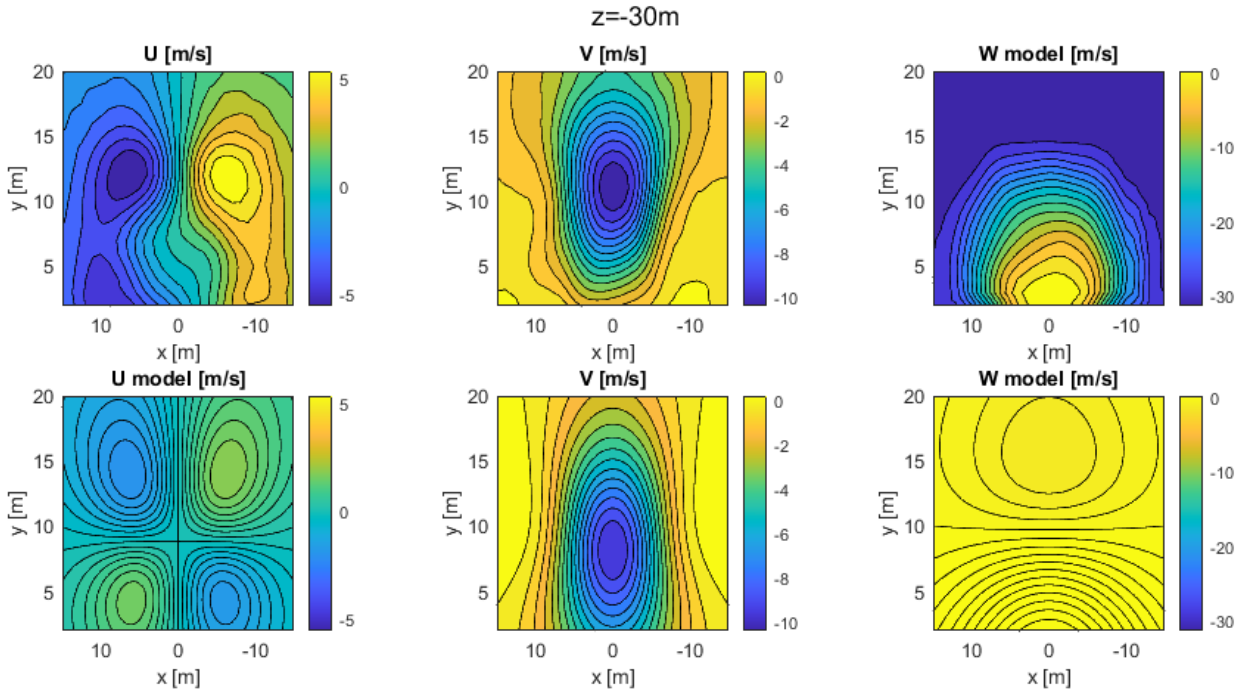

(e)

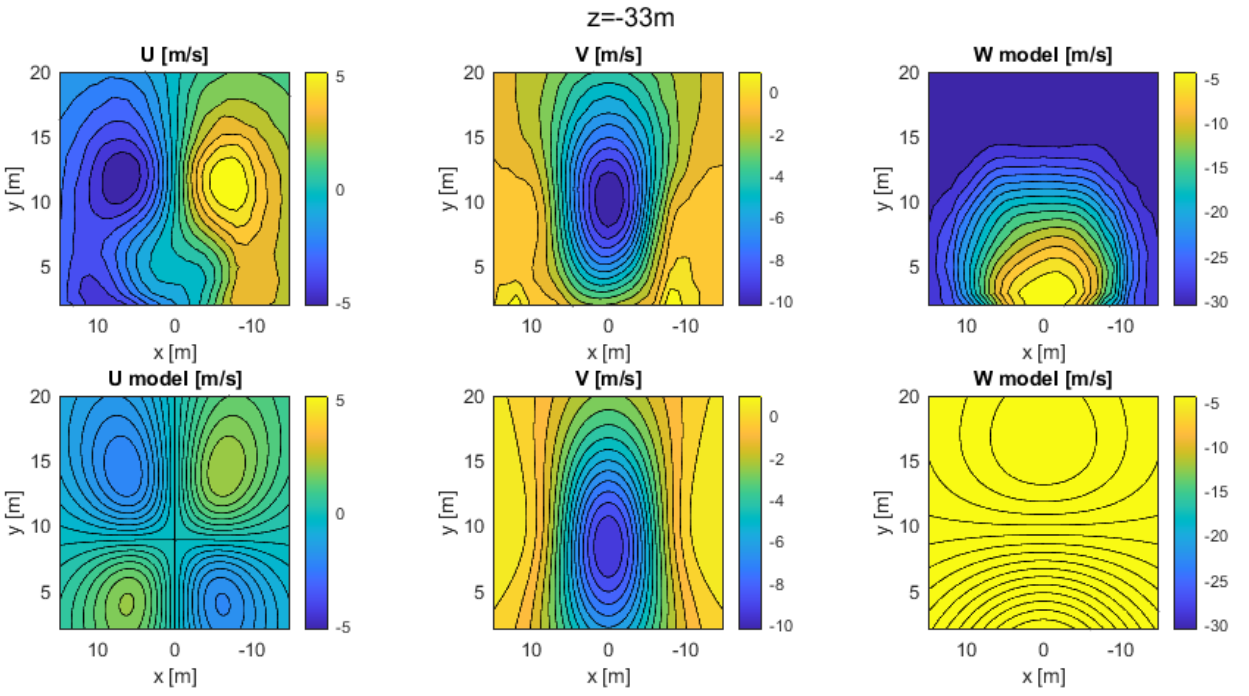

(f)

Figure 9: Contours of airwake velocity components aft of the 10m cube for various z=constant planes obtained using CGE/VorTran-M and superimposed aft arch vortex and horseshoe vortex models.

Only flow features aft of the obstacle have been considered thus far. Over the obstacle, conical vortices were noted to develop along the streamwise corner edges of the obstacle,

illustrated in Figure 10. However, upon carrying out the characterization steps listed above, these vortices were not found to be significantly potent, displaying dimensional circulation values <0.5 m^2/s. The other primary flow features over the obstacle are the separation regions that result from flow hitting the obstacle. As a simple initial attempt to account for these without having to implement a full panel code, we represented the obstacle using a vortex ring consisting of 3 straight filaments that follow the outline of the obstacle in the z=constant plane, with a corresponding ground mirror filament. We formulated and implemented an optimization problem to determine the longitudinal z-location of this vortex ring along the obstacle length, the size of the vortex core radius and the strength of the filament (the three design variables of the formulation). The objective function entailed minimizing the error in vertical velocity predictions obtained using the model and the truth data along the semi arc shown in Figure 11. The constraints consisted of lower and upper bounds on the design variables. Vertical velocity reconstruction was then carried out using Eq. (2) with $fac = 1$ to evaluate the characterization. Vertical velocity predictions along the x=0m plane are shown in Figure 12. Reasonable agreement is noted with this first cut attempt. Further refinement of the modeling is underway.

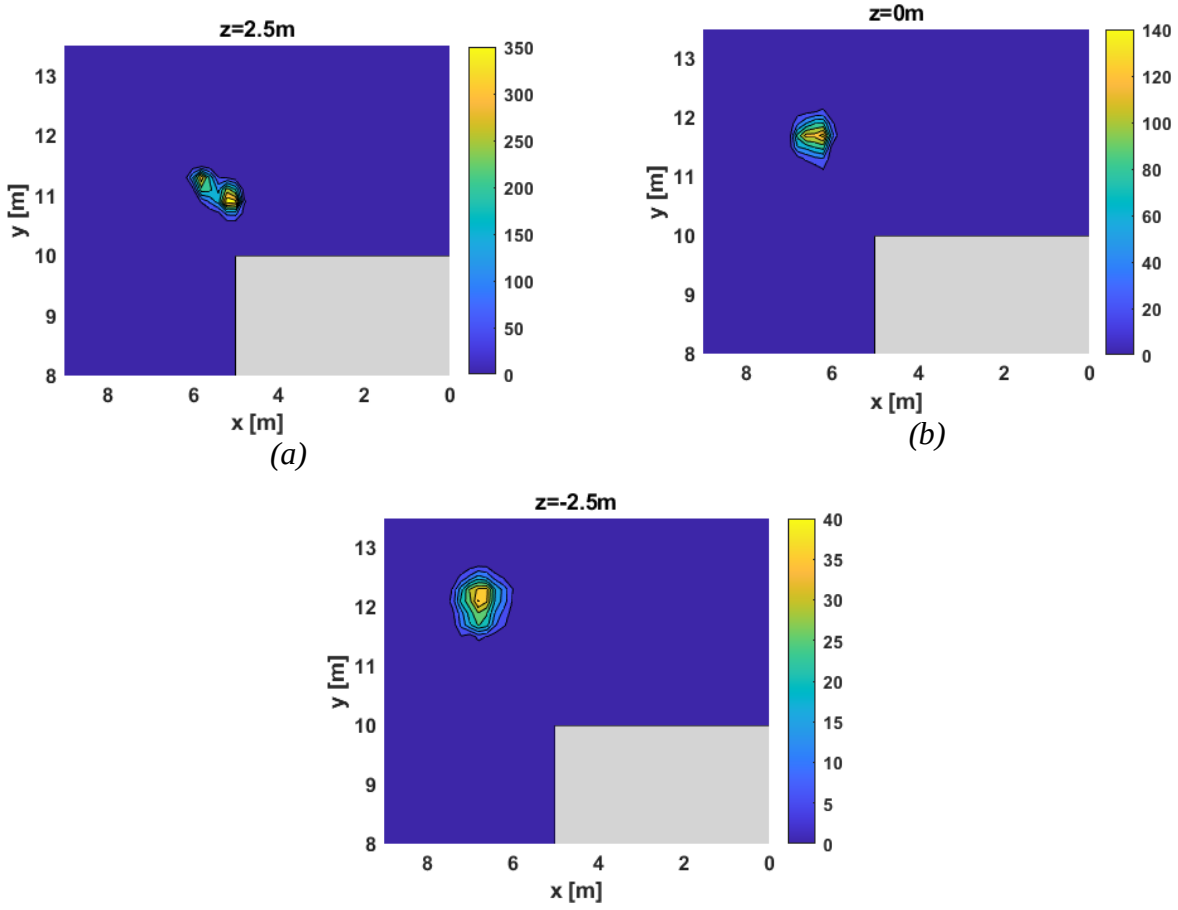

Figure 10: Contour plots of λ_2 vortex identification criterion at various z=constant planes indicated presented of moving corner vortex.

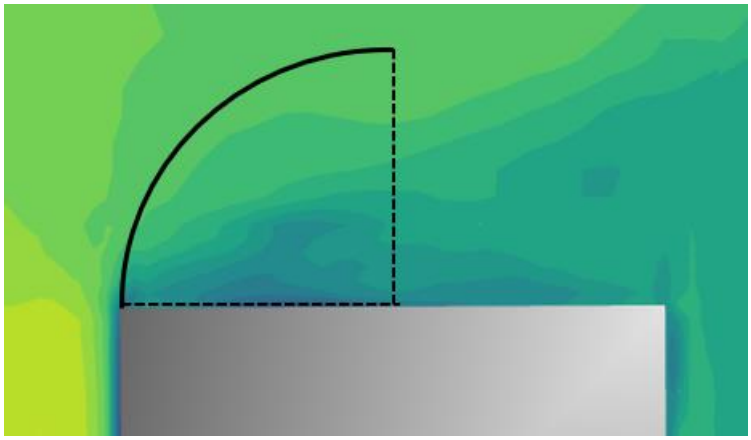

Figure 11: Illustration of arc (black solid line) along which predictions were made for optimization.

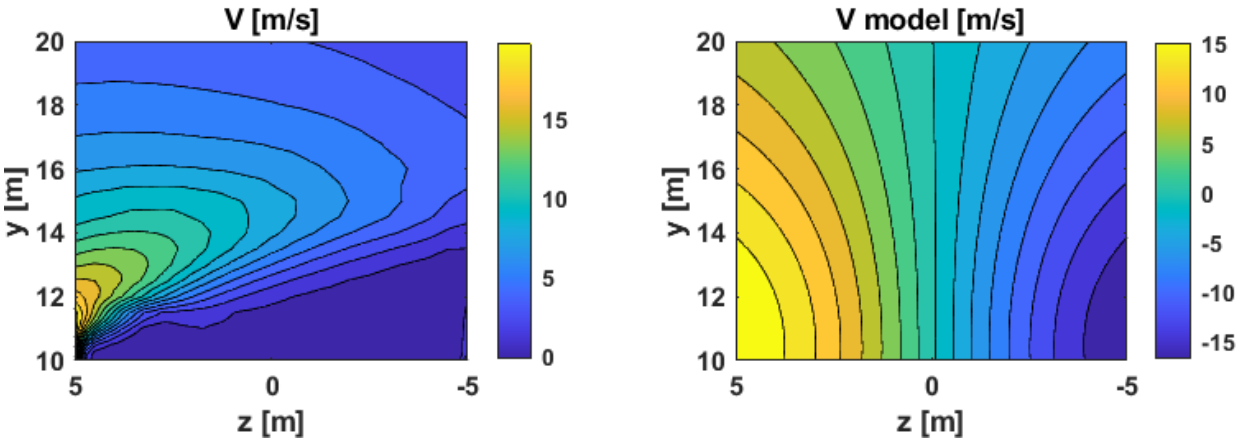

Figure 12: Vertical velocity predictions for region along x=0m plane over the top of the cube using the simplified ring vortex model for the obstacle.

We identified and performed characterization of four main flow features for headwind flow over a simple cube. These include: the arch vortex immediately aft of the obstacle, the horseshoe filament aft of the cube that extends downstream, the conical vortices along the corner edges of the obstacle (which were found to not be significantly potent) and the separation regions resulting from the interaction of freestream with the obstacle (represented in a simplified manner as a vortex ring with a ground mirror counterpart).

Generic Ship Geometry Parametrization

As a step up from analyses of flow over a cube, we consider flow over representative ship geometries. We implemented a generic geometry parametrization for ship structures shown in Figure 13. Corresponding parameters for the 5 ships shown in Figure 14 were then derived using information available in online databases. These are summarized in Table 2, where the two categories of ships are evident: flat topped ship geometries (category #1), where the superstructure does not cover the ship beam ($W \neq L_W$) and (category #2) ships where the superstructure width matches the ship beam ($W = L_W$). Nondimensional geometrical relations for the various ships are shown in Table 3, where the nondimensional parameters for the second category are relatively close to each other. In this report, we consider primarily a generic

category #2 ship geometry whose dimensions were obtained using the average of the nondimensional relations shown in Table 3, together with a scaling length of $L = 40$m. The resulting geometry is depicted in Figure 15. We performed a 30 m/s headwind simulation of flow over the resulting generic configuration and recorded transient time history data in 0.1s increments for a total of 25s for a rectangular domain of interest that is aft of the hangar and extends up to $1.4L_a$ aft of the ship in the z direction, 2.4H above the hangar in the y direction and 1.25W beyond the beam on either side in the x direction.

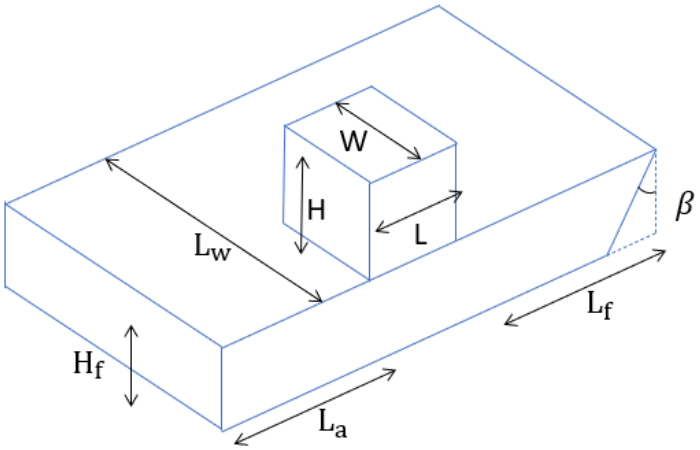

Figure 13: Generic ship geometry parameterization.

(a) CVN class ship

(b) LHD class ship

(c) LPD class ship

(d) DDG class ship

(e) LSD class ship

Figure 14: Different ship classes considered in parameterization.

Table 2: Parametrization of different ship geometries.

Geometry	L [m]	W [m]	H [m]	L_w [m]	L_f [m]	L_a [m]	H_f [m]	L_{tot} [m]	β [deg]
cube	10	10	10						
CVN	27.8	25	27.8	77	191.5	113.8	19.4	333.0	30
LHD	85.7	15	19.3	32	85.7	85.7	19.5	257.1	30
LPD	116	32	10.4	32	29.5	62.6	12.2	208.5	
DDG	64.6	20	14.2	20	43.9	46.5	7.8	155	
LSD	93	26	12.4	26	27.9	65.1	12.4	186	

Table 3: Nondimensionalization of ship geometry dimensions.

	L/W	L/H	W/L_w	H/H_f	L/L_f	L/L_a	L/L_{tot}
cube	1.00	1.00					
CVN	1.11	1.00	0.32	1.43	0.14	0.24	0.08
LHD	5.71	4.44	0.47	0.99	1.00	1.00	0.33
LPD	3.64	11.19	1.00	0.85	3.95	1.86	0.56
DDG	3.23	4.55	1.00	1.82	1.47	1.39	0.42
LSD	3.58	7.50	1.00	1.00	3.33	1.43	0.50

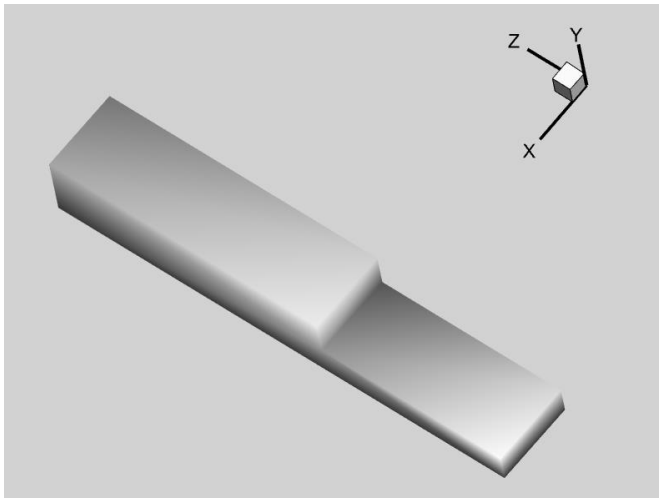

Figure 15: Rendering of generic shape geometry.

Headwind Over Generic Ship

Since the domain of interest is aft of the superstructure, we hypothesized that the arch vortex and horseshoe vortex described previously for flow aft of the cube would be applicable here as well with some corrections. In this report, we test out the scalability of the horseshoe filament since this flow feature was shown to adequately capture the vertical velocity component of ship airwake, which directly influences rotor inflow. The nondimensional spatial limits of the horseshoe vortex were dimensionalized using the ship beam ($W = 11.4\text{m}$) for x coordinates and hangar height ($H = 5.7\text{m}$) for y and z coordinates. The nondimensional circulation was dimensionalized using the freestream speed and hangar height. Figure 16 shows contours of the

velocity predictions for the horseshoe vortex obtained using Eq. (2) with $fac = 6.7$ (determined manually), together with those from CGE/VorTran-M. Note that the deck position coordinates are bounded dimensionally within $z \in [-33.33, -6.67]$m and the horizontal part of the horseshoe is at z=-14.4m. Apart from the regions near the horizontal part of the horseshoe at z=-11m and z=-15m, good agreement in lateral u and vertical v velocity predictions are noted, showcasing the scalability and applicability of this horseshoe vortex.

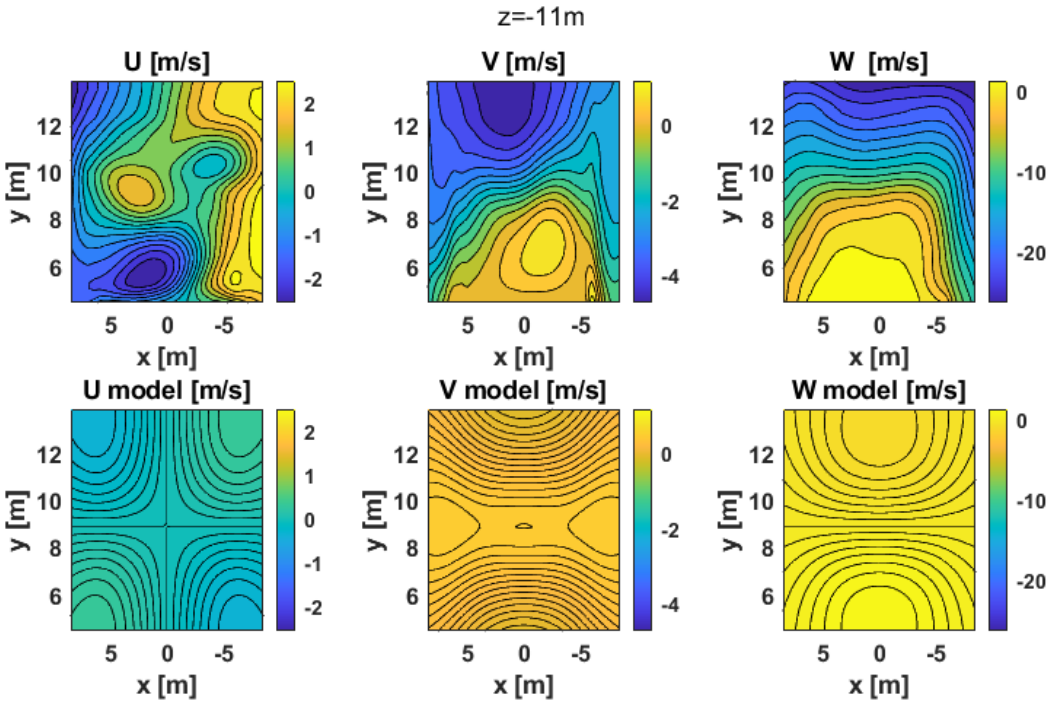

(a)

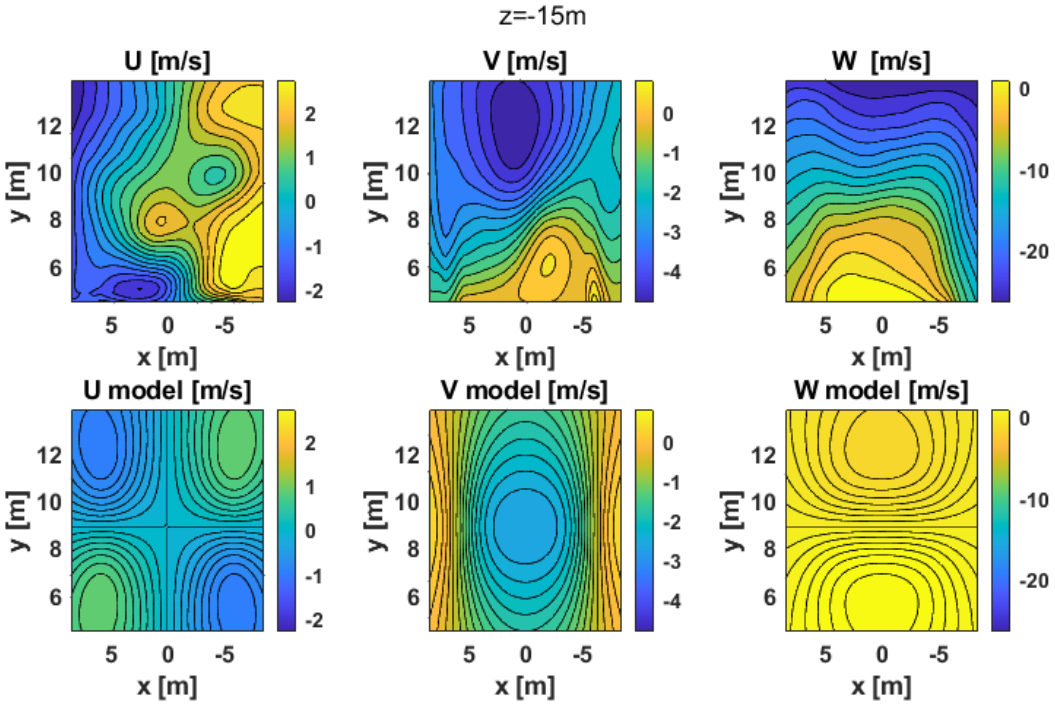

(b)

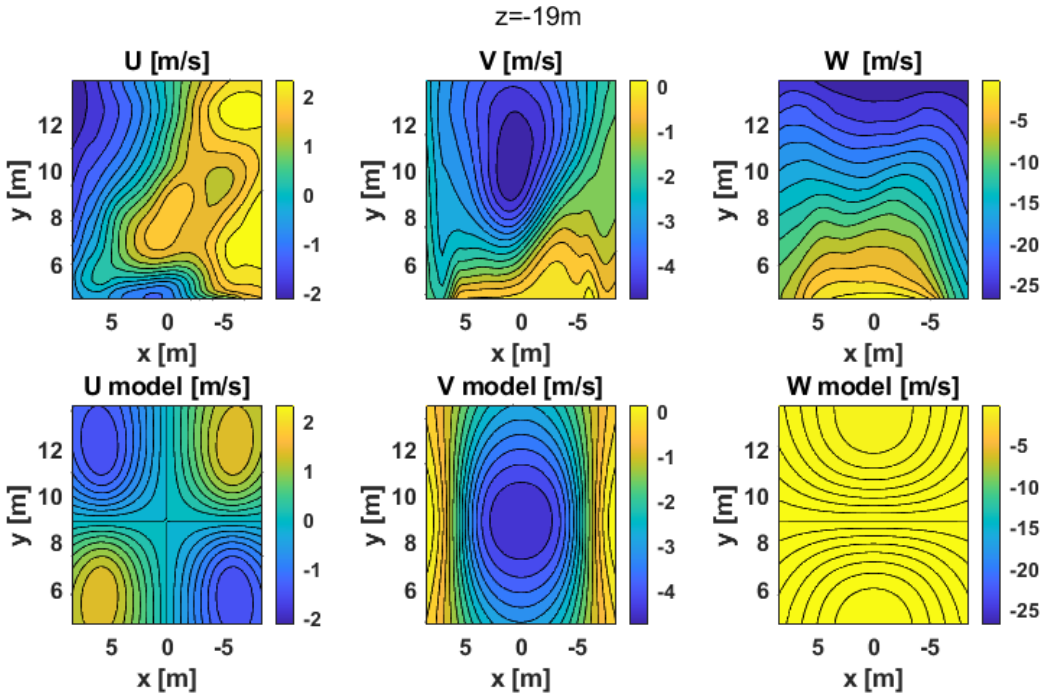

(c)

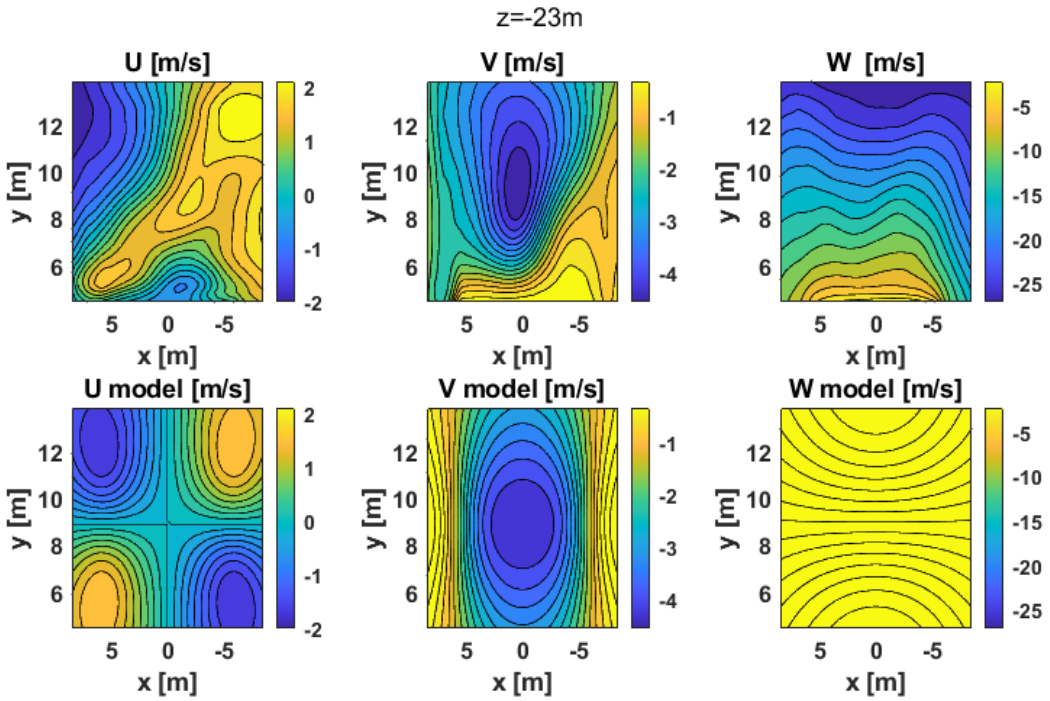

(d)

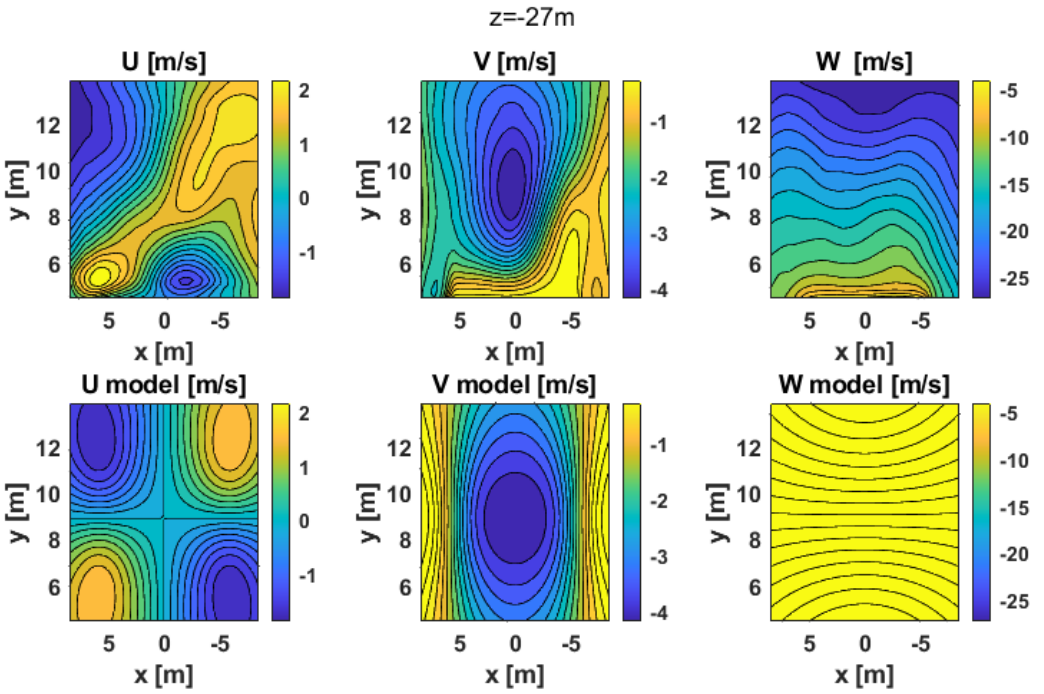
z=-27m
U [m/s]
V [m/s]
W [m/s]
U model [m/s]
V model [m/s]
W model [m/s]
y [m]
x [m]

(e)

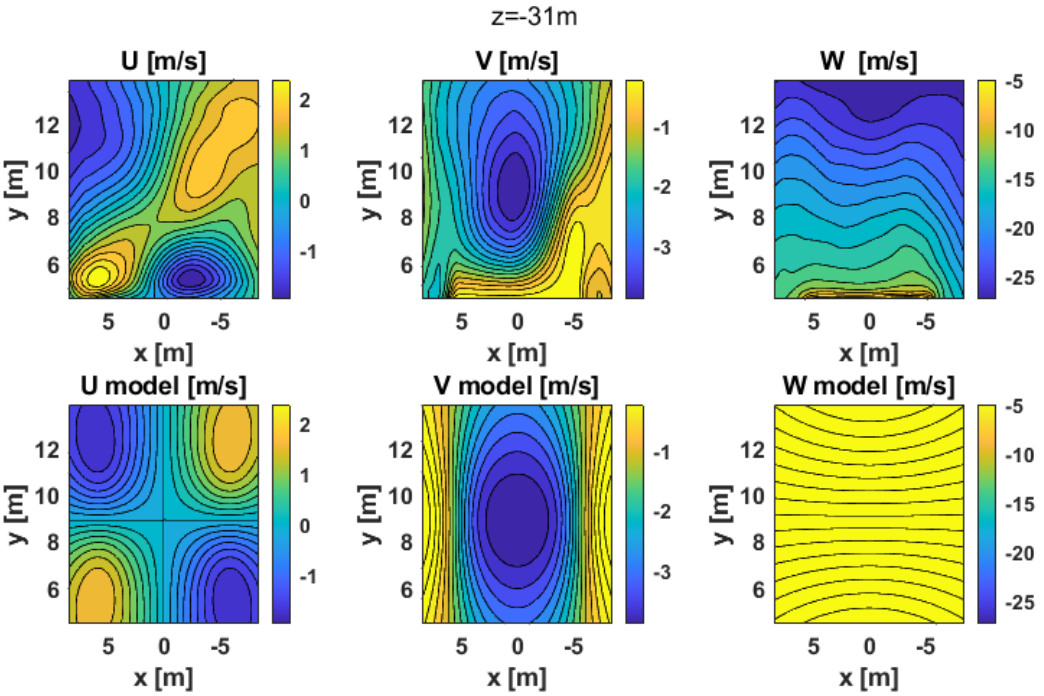
z=-31m
U [m/s]
V [m/s]
W [m/s]
U model [m/s]
V model [m/s]
W model [m/s]
y [m]
x [m]

(f)

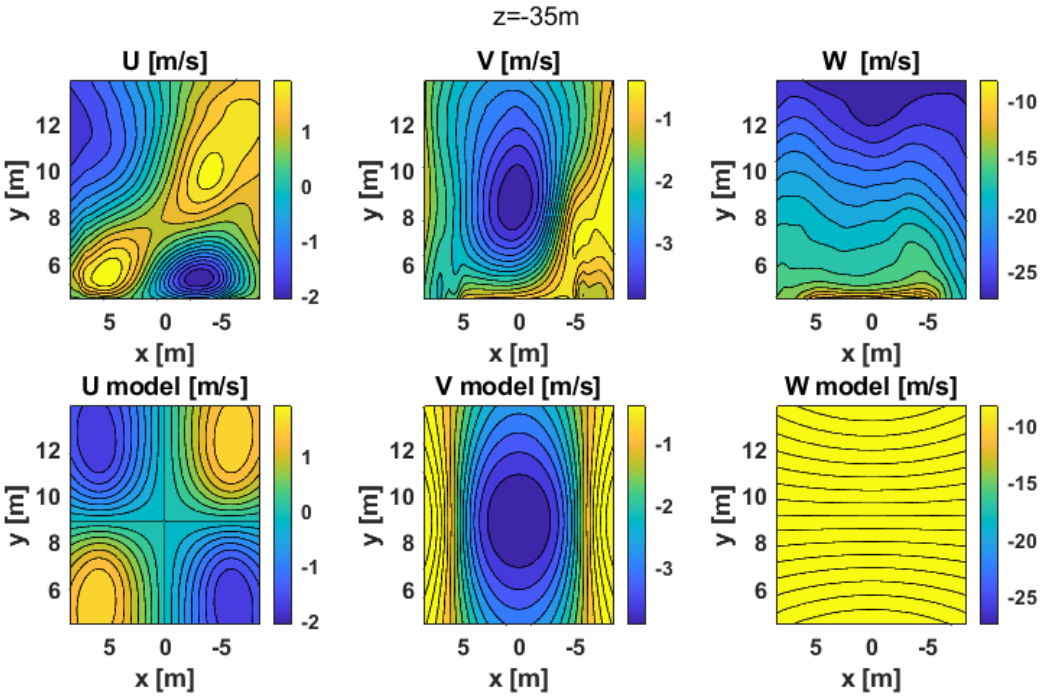

(g)

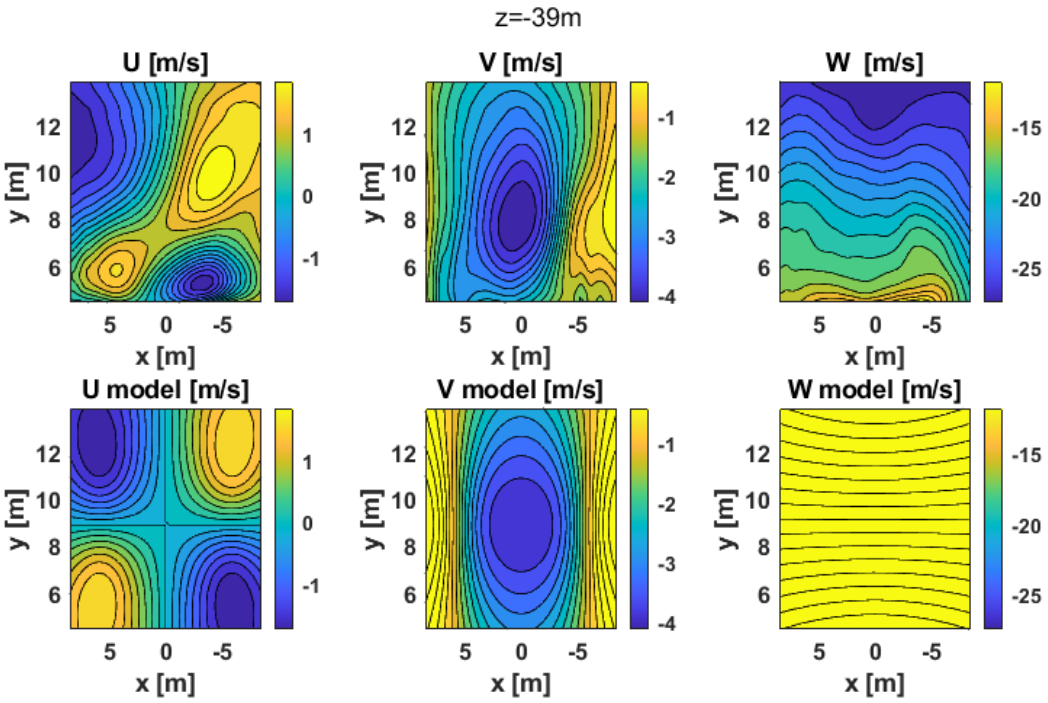

(h)

Figure 16: Contours of airwake velocity components aft of the generic ship geometry for various z=constant planes obtained using CGE/VorTran-M and aft horseshoe vortex model.

Rotor Fundamental Response in a Representative Approach trajectory

The horseshoe vortex model when implemented using Eq. (2) is equivalent to the function $v_{vortex}(r, \psi)$ from Eq. (1) and enables the computation of fundamental rotor response to the associated airwake velocities. We consider rotors representative of four helicopters as summarized in Table 1 and Figure 2. These rotors follow a straight-line approach trajectory with a constant flight path angle $\gamma = 6°$, shown in Figure 17. The rotor hub centers coincide with the ship centerline. The descent begins at an altitude $y_0 = 45.7\text{m}$ (150 ft.) with a forward speed $V_0 = 41.2\ \text{m/s}$ (80 kts), and ends in hover at an altitude $y_f = 6\text{m}$ (19.7 ft) above the center of the deck (z=-20m). We use the analytical model developed by Heffley [10] to determine the velocity and deceleration profile during this descent. This model provides velocity and deceleration expressions that are based on a human pilot's perception of the visual field during a deceleration operation from forward flight to hover and have been validated against flight test data [10]. The descent trajectory, velocity and deceleration profiles are plotted in Figure 18.

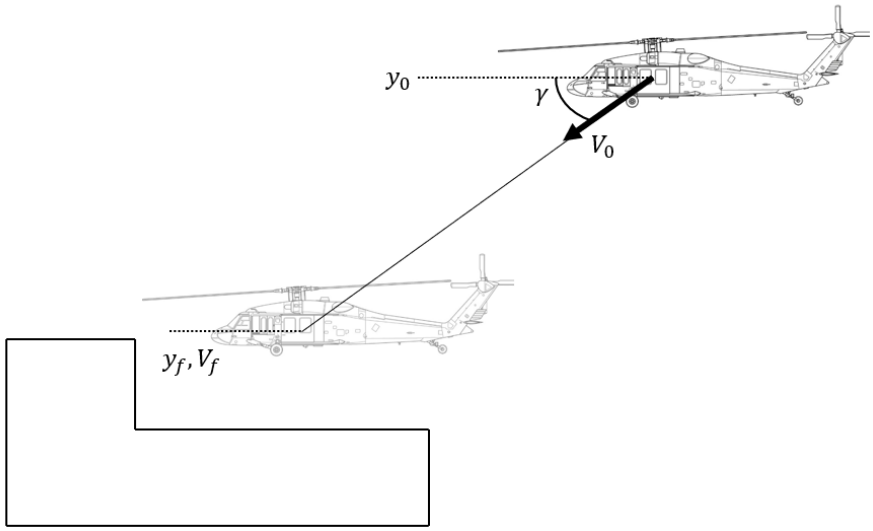

Figure 17: Illustration of approach trajectory.

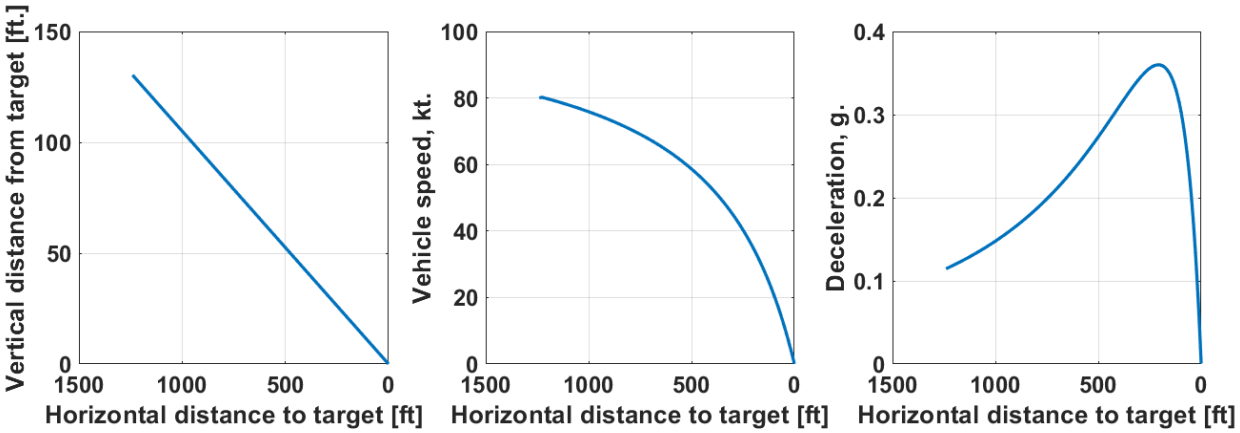

Figure 18: Approach trajectory (left), velocity (middle) and deceleration (right) profiles.

The magnitude of the horseshoe vortex influence on the thrust coefficient (C_T), disk coning (β_0) and longitudinal disk tilt (β_{1c}) as a function of nondimensional horizontal distance from the target location ($\overline{D} = D/L_a$) for the different rotors is depicted in Figure 19. Similarly, the influence of the vertical velocities obtained from CFD are given in Figure 20. Note that the change in lateral disk tilt (β_{1s}) is negligible due to symmetry of the approach and the vortex model and is thus not shown here. We make the following observations from the figures:

a. There is a steeper decrease and kinks in responses near the target location ($\overline{D} = 0$) in Figure 19 since that is close to where the horizontal part of the horseshoe vortex is situated (z=-14m).
b. In both Figures, the MQ-8C rotor experiences the greatest change in thrust coefficient, followed by the UH-60 rotor. In Figure 19, we note that the V-22 rotor experiences a slightly greater change in thrust coefficient than the CH-53E rotor, while in Figure 20 the opposite is true, with a clear distinction in the response curves. This is likely due to the influence of additional flow features in the "truth" data in Figure 20, in addition to the rotor properties and size. This difference is under further investigation.
c. A greater response in coning magnitude is noted in the truth responses in Figure 20, when compared to those in Figure 19. Apart from the CH-53E coning response, the coning response of the MQ-8C rotor is the largest, followed sequentially by that of the UH-60 rotor and the V-22 rotor in both figures, which gives further confidence in the horseshoe vortex model approach.
d. For the longitudinal tilt response, the CH-53E rotor is noted to have the largest response away from the target location for $\overline{D} \in [1,2]$ and smallest response closer to the target hover location. In both Figures, the β_{1c} response for the MQ-8C and V-22 rotors appear to overlap, with that of the UH-60 overlapping with them as well in Figure 19.

These results are encouraging and indicate further showcase the potential impact of the horseshoe vortex as a fundamental airwake flow feature that influences aircraft responses.

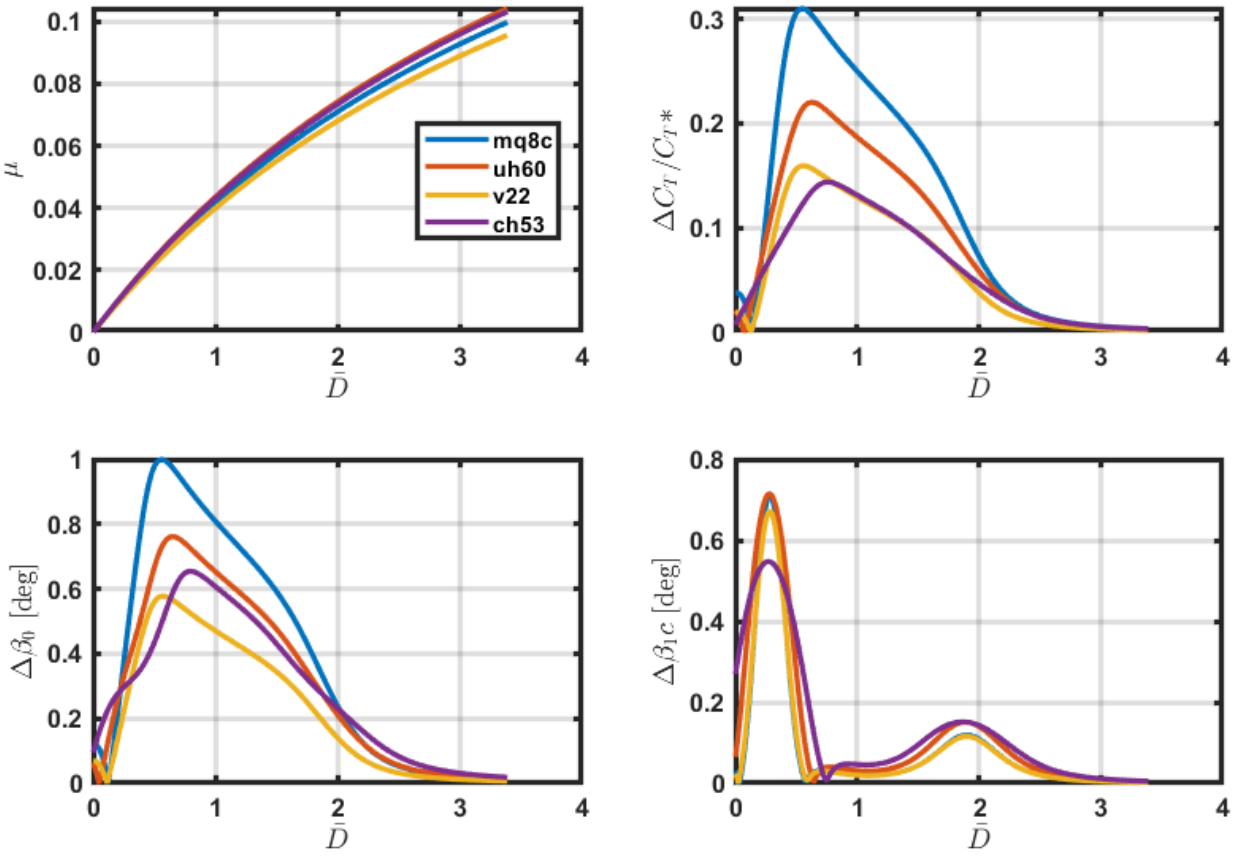

Figure 19: Advance ratio $\mu = V/\Omega R$ (top left), change in thrust coefficient (top right), change in coning (bottom left) and change in longitudinal tilt (bottom right) during approach to target hover position in the presence of horseshoe vortex; $C_T^* = W/\rho(\pi R)^2(\Omega R)^2$, $\Delta C_T = C_T - C_T^*$, $\Delta\beta_0 = \beta_0 - \beta_0^*$.

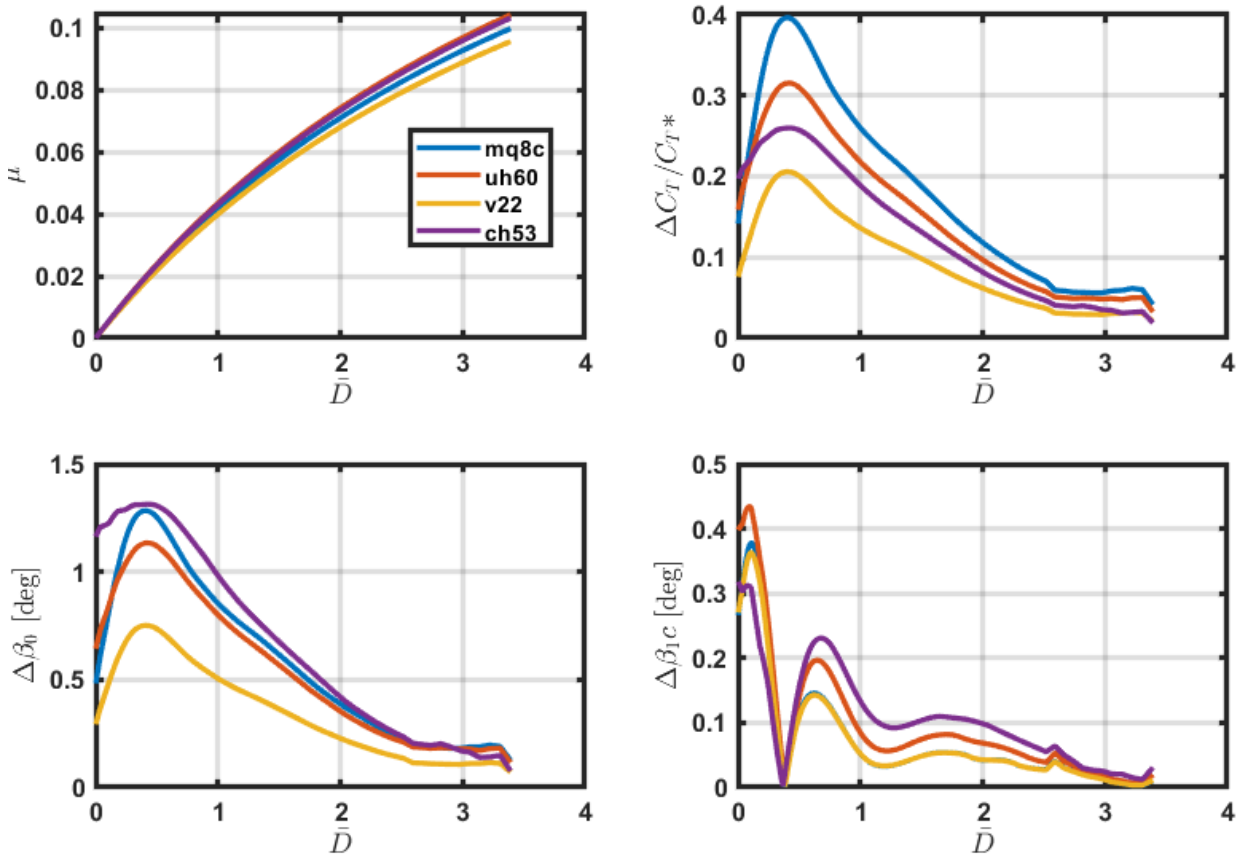

Figure 20: Advance ratio (top let), change in thrust coefficient (top right), change in coning (bottom left) and change in longitudinal tilt (bottom right) during approach to target hover position in the presence of CFD predicted vertical velocities; $C_T^* = W/\rho(\pi R)^2(\Omega R)^2$, $\Delta C_T = C_T - C_T^*$, $\Delta\beta_0 = \beta_0 - \beta_0^*$.

2023 ONR Annual Aerodynamic Program Review Slides

Establishing Fluid Dynamics Scales Critical to Dynamic Interface Applications and their Impact on Handling Qualities

FY23 ONR ONR Aerodynamics Annual Program Review

Glen Whitehouse, Abhinav Sharma and Jeffrey Keller

Continuum Dynamics, Inc.

Distribution statement A
Approved for public release: distribution unlimited

Continuum Dynamics, Inc.

July 18th 2023

Distribution Statement A
Approved for public release: distribution unlimited

Overview

- **Motivation**
- **Overall goal**
- **Background**
  - Flight Dynamics for disturbance interactions
  - Disturbance modeling
- **Questions to be answered**
- **Technical objectives and status summary**
- **Summary of work performed**
- **Plans for future work**

Motivation

- **One of the most demanding tasks for naval aviators is landing on a moving flight deck in high sea-states (i.e. the dynamic interface (DI) problem)**
- **Flight simulation has long been recognized as a valuable tool for augmenting engineering development and pilot training in DI operations**
  - Most effective when the simulation model appropriately characterizes the aerodynamic interactions between the rotorcraft and ship airwake
- **Given the complexity of the problem, a fundamental difficulty when assessing the simulation approaches is the quantification of "good enough"**
  - Understanding and predicting the underlying physics
  - Trainer fidelity (i.e. can the pilot feel/tell a difference)

Daytime and nighttime dynamic interface operations

Continuum Dynamics, Inc.

Overall Goal

- **Goal is to help quantify what is "good enough"**
  - Fundamental aero-physics of a rotorcraft interacting with an external disturbance field
  - Quantify which length and time scales directly impact the aircraft's fundamental response
  - Quantify what modeling fidelity is required to simulate interactions adequately

- **Build upon ongoing and prior efforts that seek to quantify "good enough"**
  - UMD/GIT focused on understanding the response of a wing to the wake shed by canonical structures
  - NAVAIR - Generalized Airwake Goodness Evaluation - sought to represent the entire DI scenario
  - Whitehouse and Brown looked at wake and disturbance modeling effects for a canonical isolated rotor
  - Wachspress, McKillip et al looked at developing a flight dynamics model for nearfield operations
  - Silva, Wachspress et al looked at flight dynamics of tiltrotor formation flight interactions

- **Outcomes would enable the community to establish**
  - The level of modeling fidelity required to adequately simulate disturbance interactions
  - CFD output requirements for ship airwake databases
  - Guidance that can be used to assist in specification of flying qualities, and aircraft performance requirements, such as ADS-33, DIPES and CETI

Background: Flight Dynamics Modeling

- **Estimating the response of rotorcraft to gusts, atmospheric turbulence and disturbance fields has roughly followed "best practices" from fixed-wing community**
  - Frozen field superposition
  - Assumes that time scales of the interaction are too short for mutual fluid dynamic interaction to occur

- **Early flight dynamics disturbance interaction investigation focused on**
  - Dynamic stability of the rotor
  - 1st order estimates of heave response to quantify ride quality
  - Estimates of stability derivatives for flight dynamics applications
    - Challenging to decompose aerodynamic derivative "gains" associated with only the gusts

- **Modern approach**
  - Component build-up model of the aircraft
  - Representation of aerodynamic components of the aircraft
    - Momentum theory and look-up table based models still most prevalent
    - Some demonstration cases using CFD (but rarely used due to time/computing constraints)
    - Effective state of the art is lifting surface model with a lagrangian wake and a panel method representation of the airframe

Continuum Dynamics, Inc.

Background: Disturbance Modeling

- **Frequency domain statistical representation (following frozen disturbance fixed-wing paradigm)**
  - von Karman spectra
  - Dryden "white noise"
  - Jones' Statistical Discrete Gust method
- **With the adoption of blade-element based aerodynamics models**
  - 3D lookup table
  - 4D lookup table
  - But usually superposition and frozen field
- **Distorting field (research)**
  - Limited CFD investigations at NAVAIR and by Whitehouse and Brown (see next slide)
  - Particle method wake interacting with a lagrangian rotor wake (CDI)
  - To date, usually limited to "proof-of-concept" or specific/limited applications

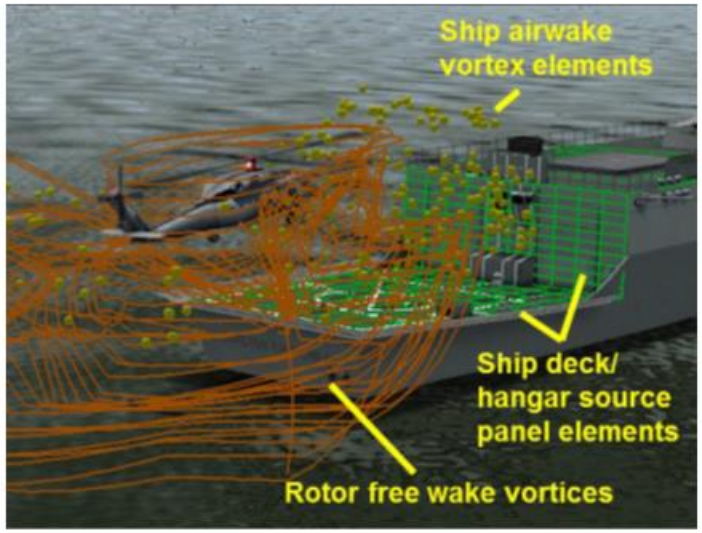

CASTLE / ExHel / CHARM visualization of shipboard operations

Continuum Dynamics, Inc.

Background: Disturbance Modeling (cont'd)

- **Distortion of the wake and the disturbance can result in significant changes in aeromechanics**
  - Function of "interaction time"
  - Function of relative strength
- **Whitehouse and Brown investigated wake and disturbance modeling assumptions**
  - Intention here is to build upon Whitehouse and Brown and work elsewhere to understand how these observations apply to more general cases

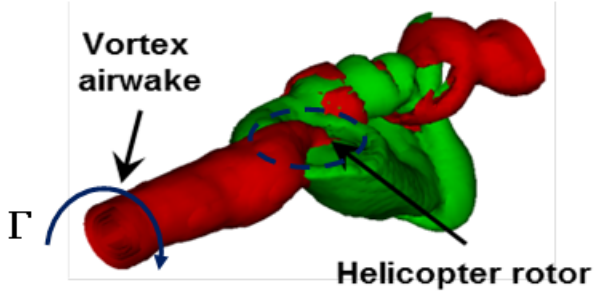

Wake distortion for a "parallel" wake vortex interaction

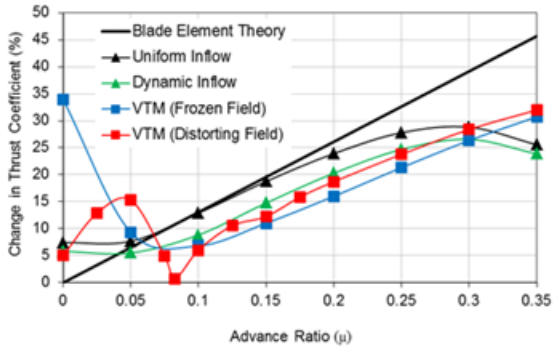

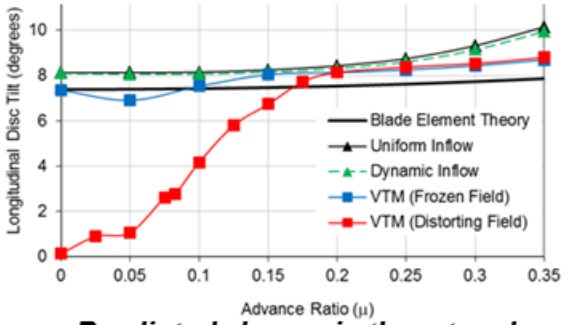

Predicted change in thrust and longitudinal flapping as a function of forward speed for a "parallel" interaction

Continuum Dynamics, Inc.

Questions to be Answered

1. **What spatial and temporal scales, present in a disturbance field, matter from Flight Dynamics and Flying Qualities standpoints?**
   - Beyond the obvious constraints (i.e. larger than a rotor radius and those that induce velocities larger than the wake induced velocity)

2. **How do these scales vary when the full aircraft is accounted for?**
   - Helicopter response dominated by that of the rotor
   - May still be significant response associated with the fuselage, empennage and tail rotor

3. **How do these scales vary with aircraft configuration/type?**
   - Rotor response is ~90° out of phase
   - Wing response is in phase
   - Integrated response also a function of nacelle angle for tiltrotor

4. **How do these scales vary with aircraft flight condition, and can modeling simplifications be made without fundamentally changing the response?**
   - e.g. is frozen field assumption acceptable above a certain speed?

Technical Objectives and Status Summary

- **Define spatial and temporal fluid dynamic scales and develop numerical representations**
  - Identified types of primary flow features in relevant disturbance fields
  - Numerical simulation and simplified model development ongoing
- **6-DOF generic flight dynamics model assembly and testing**
  - Received approval to use NAVAIR's CASTLE simulation environment with example helicopter and tiltrotor models
  - Re-hosting and reintegrating CHARM with these models and confirming operation
- **Define aeromechanics performance and FQ metrics, and simulation test matrix**
  - Underway
- **Undertake simulation of a rotorcraft interacting with disturbance fields**
  - Focus of coming year

Summary of Work Performed

- **Definition of Disturbance Field Scales Relevant to Naval Rotorcraft Operations**
  - Usually think of problem in a quasi-steady manner
  - Unsteady and frequency content is also important
    - Pilot workload usually associated with responses in the 0.2-2Hz (1-10rad/s) range
  - Literature review was conducted to identify relevant flow features and how these features have been quantified

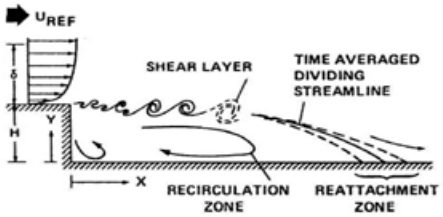

2D backward-facing step *(Driver et al, 1987)*

- St≈0.2
- Peak turbulence of I=20% (Eaton & Johnston, 1981)

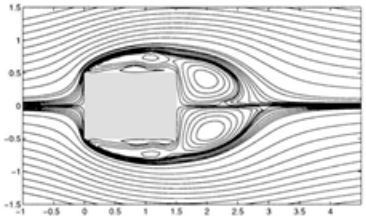

2D shear layer *(Okajima, 1982)*

- St≈0.2
- Bluff body shape/size influences reattachment location

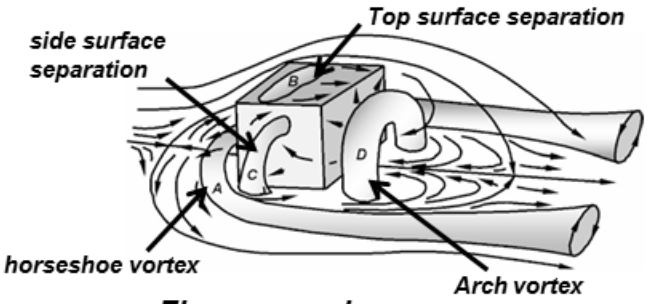

Flow over cube *(Sousa, 2002)*

- 3D effects prominent
- St ≈ 0.104

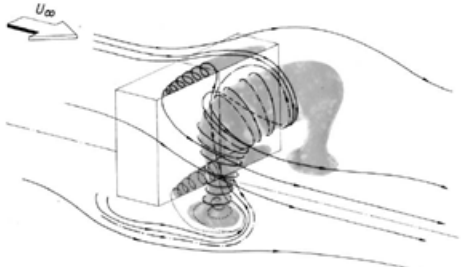

Flow over rectangular prism *(Becker et al., 2002)*

- Frequency and length scales are proportional to prism dimensions

Continuum Dynamics, Inc.

Summary of Work Performed (cont'd)

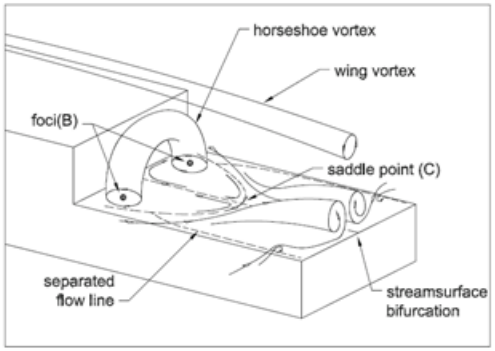

Double-backward facing step *(Tinney & Ukeiley, 2009)*

- Representative of a ship deck
- Frequency scales based on St ≈ 0.17
- Peak longitudinal turbulence intensity I = 20% noted near deck center (Forrest & Owen, 2010)

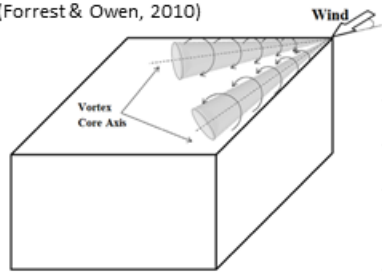

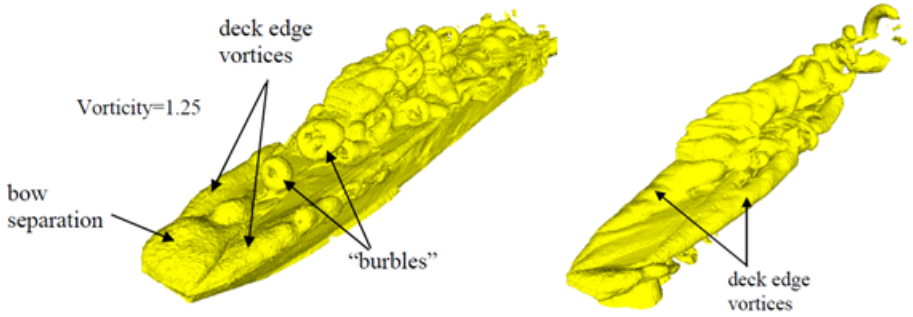

Flat-topped aircraft carrier *(Polsky & Bruner, 2003; Rajagopalan et al., 2005)*

- Burbles shed at St_h ≈ 0.26-0.38 in headwind
- Highly turbulent region aft of superstructure
- Deck-edge vortices allowed to spread over deck and in oblique conditions can produce large lateral disturbance velocities

Corner vortices *(Mooneghi & Kargarmoakhar, 2016)*

- Similar to wing/deck-edge vortices
- Produce high suction regions near surface
- Vortex size depends on obstacle dimensions, wind speed, incidence angle with corner and upstream turbulence
- Limited studies on velocity distribution above surface

Continuum Dynamics, Inc.

Distribution statement A Slide 11

Summary of Work Performed (cont'd)

- **Additional Findings**
  - Ship motion can cause the vortex shedding to "lock in" with ship motion frequency
  - Flow features of interest broadly categorized as
    - Shear layers shed from edges of bluff body obstacles
    - Deck-edge/wing vortices that develop due to pressure gradients between side and top surfaces
    - Corner vortices that originate in oblique wind-over-deck conditions
  - Characterization of relevant vortical structures in terms of Strouhal number and unsteady characterization in terms of turbulence intensity and turbulent kinetic energy available but information on strength of vortices not readily found in literature

- **Generation of Synthetic Disturbance Fields**
  - Simplified airwake models being developed using time-accurate CFD simulations of flow over cube as starting point (CDI's CGE/Vortran-M code used for simulations)
  - Formulation entails fitting 2D analytical vortex models on primary flow features and subsequently superimposing them to reconstruct airwake velocities
  - Paves way for parametrization and scaling such that airwake around different ship geometries may be obtained by simply modifying inputs to the vortex models
  - Characterization of flow features in terms of geometry and strength also underway

Summary of Work Performed (cont'd)

- **Initial results for top surface separation**
  - 2D vortex model proposed by Banks & Meroney, 2001 for corner vortices modified for use
  - Vortex model can be thought of as wheel spinning due to free stream
  - Modified model provides piece-wise continuous functions of longitudinal velocity profile at any span location over top surface
  - 3 inputs: vortex radius, location of spin point M, and spin velocity

Illustration of vortex model
(Banks & Meroney, 2001)

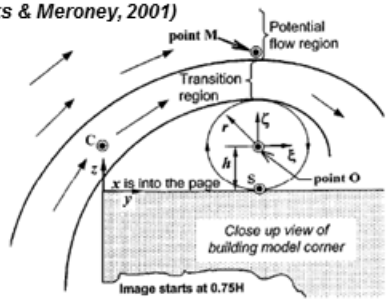

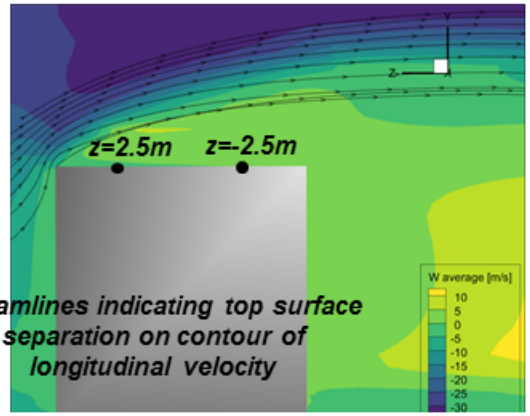

Streamlines indicating top surface separation on contour of longitudinal velocity

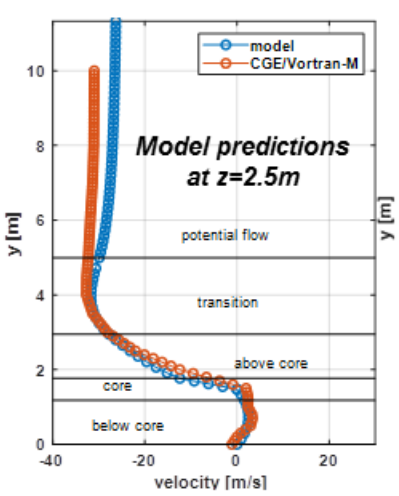

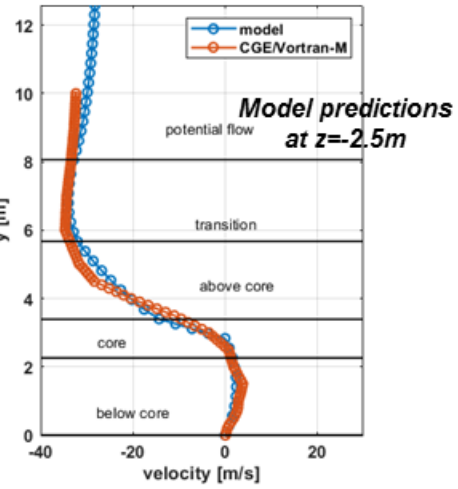

Continuum Dynamics, Inc.

Summary of Work Performed (cont'd)

- **Refined model for longitudinal velocity predictions aft of obstacle**
  - 1D extended to 2D planar model using polynomial relations
  - 3D velocity reconstruction achieved via interpolation
- **Model further refined and generalized for scalability**
  - Generalized polynomial expressions for model input parameters derived and nondimensionalized using freestream and geometry dimensions
  - Expressions found to be applicable for two additional rectangular configurations
    - 3x wider configuration (width is perpendicular to headwind)
    - 7x longer configuration (length is parallel to headwind)
- **Similarly scalable model being developed for vertical velocity**

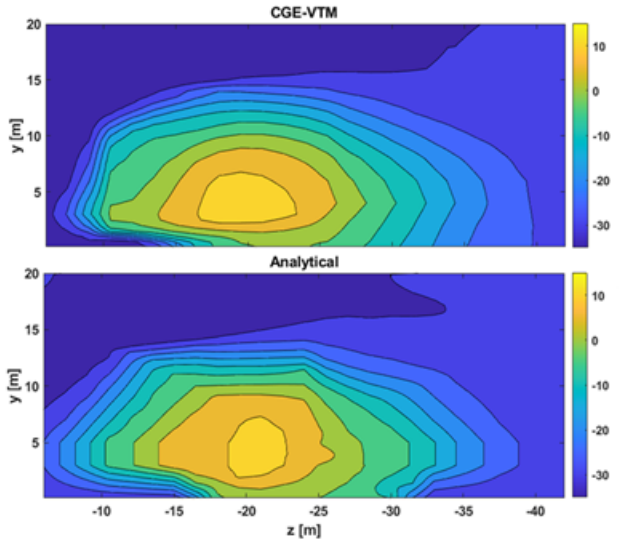

Model predictions compared to CFD on transverse downstream slice

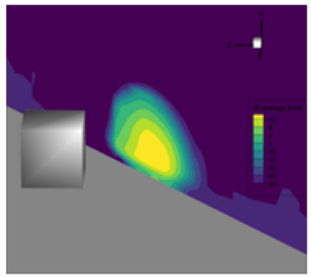

Continuum Dynamics, Inc.

Summary of Work Performed (cont'd)

- **Flow feature characterization**
  - Characterization of key flow features in terms of geometry (position/size) and strength underway
  - Arch vortex aft of rectangular prisms considered using time-averaged velocities
    - Parabolic vortex filament with ground mirror filament (nondimensional polynomial relations derived using flow aft of cube as basis)
    - Biot-Savart law combined with Vastistas core model used to test out characterization
    - Characterization found to be applicable for rectangular prism that is 3x wider highlighting scalability potential

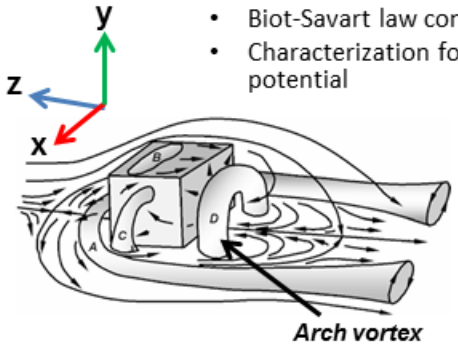

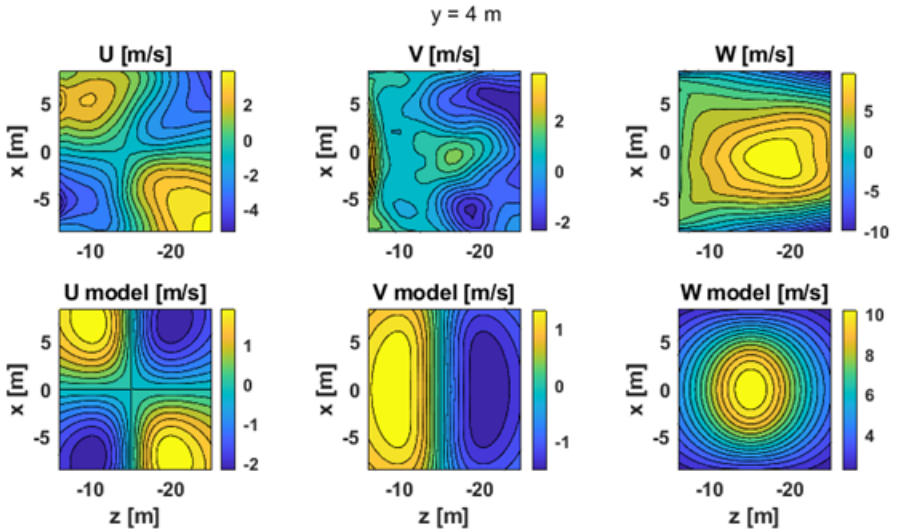

Velocity predictions on a slice plane aft of a 10m cube in the presence of a 30m/s headwind

Continuum Dynamics, Inc.

Distribution statement A 15

Summary of Work Performed (cont'd)

- **Rotor fundamental response**
  - Goal is to get rough scaling baseline for given types of disturbance to help guide future analyses
  - Derivation follows Whitehouse & Brown 2003
    - Isolated, centrally-hinged rotor with fixed controls
    - Quasi-static response with no hub accelerations
    - BET and vertical component of disturbance
    - Supports arbitrary disturbances, but may require numerical integration

$$C_T = C_T^* - \frac{Nca}{4\pi^2}\int_0^{2\pi}\int_0^1 v_{vortex}(r,\psi)(r+\mu\sin\psi)dr\,d\psi$$

$$\beta_0 = \beta_0^* - \frac{ca}{4\pi^2\omega^2 I_\beta}\int_0^{2\pi}\int_0^1 v_{vortex}(r,\psi)(r^2+\mu r\sin\psi)dr\,d\psi$$

$$\beta_{1s} = \beta_{1s}^* + \frac{ca}{2\pi^2(\omega^2-1)I_\beta}\int_0^{2\pi}\int_0^1 v_{vortex}(r,\psi)(r^2\sin\psi+\mu r\sin^2\psi)dr\,d\psi$$

$$\beta_{1c} = \beta_{1c}^* + \frac{ca}{2\pi^2(\omega^2-1)I_\beta}\int_0^{2\pi}\int_0^1 v_{vortex}(r,\psi)(r^2\cos\psi+\mu r\cos\psi\sin\psi)dr\,d\psi$$

a = lift-curve slope
c = chord, scaled by R
r = radial coordinate, scaled by R
v_{vortex} = vortex velocity function
N = number of blades
R = rotor radius
C_T = Thrust coefficient
β_0 = rotor coning
β_{1c} = rotor longitudinal tilt
β_{1s} = rotor lateral tilt
ψ = rotor azimuth
ω = flap natural frequency, scaled by rotor rotational speed
$(\,)^*$ = response without vortex

"Whitehouse, G. R., and Brown, R. E. "Modeling The Mutual Distortions of Interacting Helicopter and Aircraft Wakes." Journal of Aircraft, Vol. 40, No. 3, 2003, pp. 440–448. https://doi.org/10.2514/2.3139

Summary of Work Performed (cont'd)

- **Rotor fundamental response (cont'd)**
  - Use simple model for the 10m cube as a basis (same as earlier model results)
    - 3D curved vortex model
  - Look at isolated rotor response for range of relevant rotor sizes
    - MQ-8c Fire Scout (R=17.5ft)
    - V-22 (19ft)
    - SH-60 (R=26.83ft)
    - CH-53E (R=39.5ft)
  - Rotor at
    - 8m altitude, 10 downstream (location #1)
    - 6m altitude, 15 downstream (location #2)

"Whitehouse, G. R., and Brown, R. E. "Modeling The Mutual Distortions of Interacting Helicopter and Aircraft Wakes." Journal of Aircraft, Vol. 40, No. 3, 2003, pp. 440–448. https://doi.org/10.2514/2.3139

Continuum Dynamics, Inc.

Summary of Work Performed (cont'd)

- **Rotor fundamental response (cont'd)**

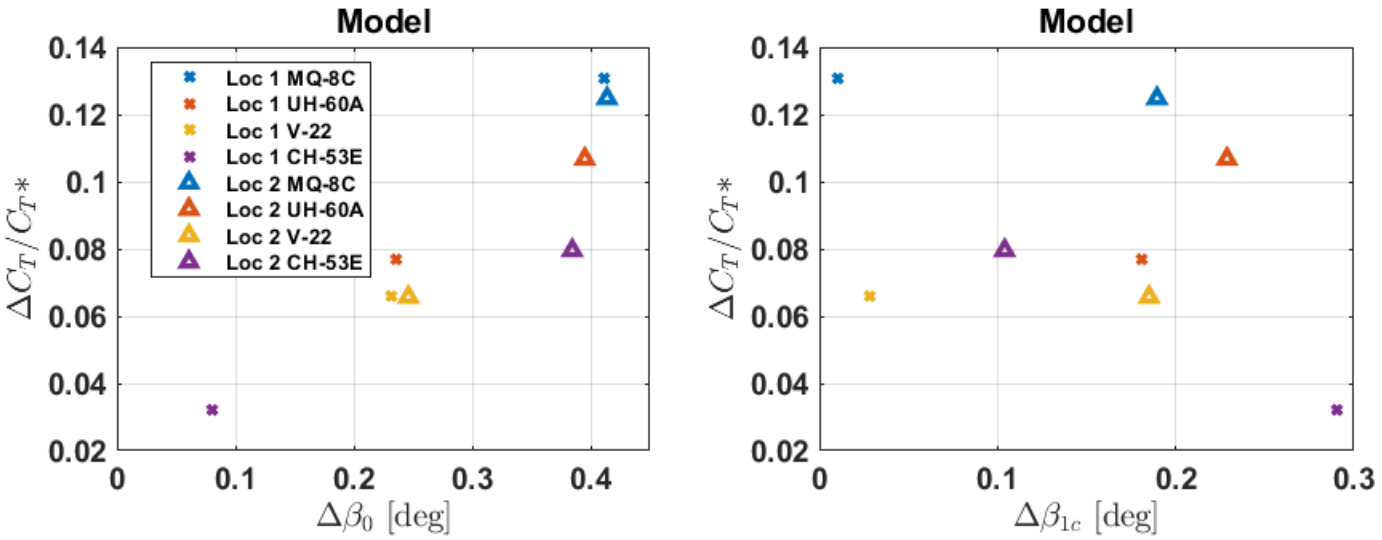

Lateral tilt $\Delta\beta_{1s}$ response negligible in this case

Continuum Dynamics, Inc.

"Whitehouse, G. R., and Brown, R. E. "Modeling The Mutual Distortions of Interacting Helicopter and Aircraft Wakes." Journal of Aircraft, Vol. 40, No. 3, 2003, pp. 440–448. https://doi.org/10.2514/2.3139

Plans for Future Work

- **Evaluation of Fundamental Helicopter Response**
  - Fixed controls, with constrained motion for "worst case"
  - Configuration permutations
    - Isolated main rotor
    - Main rotor and tail rotor
    - Rotors and fuselage (lookup table)
    - Rotors and fuselage (panel method for the fuselage)

- **Evaluation of Fundamental Tiltrotor Response**
  - Fixed controls, with constrained motion for "worst case"
  - Repeat permutations above, but also include the wing

- **Evaluation of Helicopter Flight Dynamics Response**
  - Aircraft specific properties (e.g. weight, control system etc.) where aircraft can move
  - Repeat permutations above

- **Evaluation of Tiltrotor Flight Dynamics Response**
  - Aircraft specific properties (e.g. weight, control system etc.) where aircraft can move
  - Repeat permutations above, but also include the wing

Continuum Dynamics, Inc.

Summary

- **Flight simulation is a valuable tool for engineering development and pilot training**
  - Most effective when the simulation model appropriately characterizes the interactions
- **How do we know if model "appropriately characterizes the interactions"?**
  - Underlying physics
    - Do we understand the phenomena and can we predict the physics?
  - Trainer fidelity
    - Can we implement sufficient fidelity and can the pilot feel/tell a difference?
- **Goal of this effort is to quantify what is "good enough"**
  - Fundamental aero-physics of a rotorcraft interacting with an external disturbance field
  - Quantify which length and time scales directly impact the aircraft's fundamental response
  - Quantify what modeling fidelity is required to simulate interactions adequately
- **Outcomes would enable the community to establish**
  - The level of modeling fidelity required to accurately simulate disturbance interactions
  - Guidance that can be used to assist in defining requirements for trainers, training, flying qualities and handling qualities

Continuum Dynamics, Inc.

Acknowledgements

This material is based upon work supported by the Office of Naval Research under Contract No. N00014-21-C-1044.

Any opinions, findings and conclusions or recommendations expressed in this material are those of the author(s) and do not necessarily reflect the views of the Office of Naval Research.

Plans for the Next Reporting Period

In the next reporting period, we will build upon the understanding of the types of flowfields experienced by naval aviators described previously and continue to quantify the scales and nature of the relevant primary flow structures. Characterization of ship airwake flow features as vortical structures in terms of size and strength is an aspect that does not seem to have been examined in literature. In this reporting period, we supplemented the initial characterization we had performed for the arch vortex noted aft of rectangular obstacles (representative of simplified ship superstructures) for headwind flow by considering additional flow features both aft and over the obstacles. We introduced a generic ship geometry parametrization and demonstrated the scalability and applicability of one of the flow structures identified with the rectangular obstacle with this new configuration. We subsequently examined the influence of this flow feature on the fundamental response of rotors representative of four different classes of rotorcraft, including the MQ-8C, UH-60A, V-22 and CH-53E. These rotors followed an approach trajectory representative of typical rotorcraft approaches. In the subsequent reporting period, we will perform similar characterization of additional ship airwake flow features and examine the viability of superposition to adequately represent airwake associated with different ship geometries. We will also consider aircraft response in terms of additional parametrizable and scalable metrics beyond aircraft fundamental response, and we will continue work on the development of scalable analytical models for full airwake reconstruction. As mentioned in the prior report, CHARM has been fully integrated with CASTLE and the V-22 model. During the next period of performance we will complete integration with the Example Helicopter Model and confirm operation. Development of representative "canonical" surrogate flowfields will continue, and we will work on testing them out in CASTLE simulations.

References

1. Smith, M.J., A. Jones, A. Grubb, and J. Lefebvre. *Identification and Quantification of the Role of Turbulence in Aircraft/Ship Aerodynamics*. *ONR Annual Review*. 2020. Arlingon, VA.
2. Silva, M.J., D.A. Wachspress, D.P. Gaublomme, E.W. Hayden, T.S. Davis, and T. Fean. *The Role of Modeling & Simulation in the Mitigation of V-22 Tiltrotor Formation Flight Wake-Induced Roll-off. 72nd Annual Forum of the American Helicopter Society*. 2016. West Palm Beach, FL.
3. Whitehouse, G.R. and R.E. Brown. *Modelling a Helicopter Rotor's Response to Encounters with Aircraft Wakes*. in *28th European Rotorcraft Forum*. 2002. Bristol, UK.
4. Whitehouse, G.R. and R.E. Brown. *Helicopter Rotor Response to Wake Encounters in Ground Effect*. in *59th Annual Forum of the American Helicopter Society*. 2003. Phoenix, AZ.
5. Whitehouse, G.R. and R.E. Brown, *Modelling the Mutual Distortions of Interacting Helicopter and Aircraft Wakes.* Journal of Aircraft, 2003. **Vol. 40**(No. 3): p. pp. 440-449.
6. Whitehouse, G.R. and R.E. Brown, *Modelling a Helicopter Rotor's Response to Wake Encounters.* The Aeronautical Journal, 2004. **Vol. 108**(No. 1079): p. pp. 15-26.
7. Whitehouse, G.R., *Helicopter Response to Vortex Encounters in the Near-Airfield Environment*, 2003, PhD Thesis, Department of Aeronautics Imperial College London.
8. ADS-33E-PRF. *Aeronautical Design Standard Performance Specification Handling Qualities Requirements for Military Rotorcraft*. in *US Army Aviation and Missile Command, Aviation Engineering Directorate*. 2000. Redstone Arsenal, Alabama.

9. Sousa, J.M.M., *Turbulent Flow Around a Surface-Mounted Obstacle Using 2D-3C DPIV.* Experiments in Fluids, 2002. **Vol. 33**(No. 6): p. pp. 854-862.
10. Heffley, R.K. *A Model for Manual Decelerating Approaches to Hover*. *15th Annual Conference on Manual Control*. 1979. AFFDL-TR-79-3134.